Electronic Supplementary Material (ESI) for ChemComm.

Supporting Information

Halogen Bonding Between Metal Center and Halocarbon

Daniil M. Ivanov,[†] Alexander S. Novikov,[†] Ivan V. Ananyev,[‡] Yulia V. Kirina,[†] Vadim Yu. Kukushkin*,[†]

[†] *Institute of Chemistry, Saint Petersburg State University, Universitetskaya Nab., 7/9, 199034 Saint Petersburg, Russian Federation*

[‡] *Institute of Organoelement Compounds, Russian Academy of Sciences, Vavilova St., 28, 119991 Moscow, Russian Federation*

SUPPORTING INFORMATION

PART 1. RESULTS OF XRD EXPERIMENTS

XR1. Comparison of the bond lengths of the *trans*-bis(dialkylcyanamide)Pt^{II} complexes in unsolvated solids and in the associates

Table 1S. Structure numbering, solvent systems, and quality of X-ray data (*R* values).

X	R_2	Number	Solvent	Structure	*R*, %
Cl	Me_2	**1a**	$CHCl_3$	**1a**[a]	3.04
			$CHCl_3$	**1a**•½$CHCl_3$•1½CHI_3	2.72
			CH_2Cl_2	**1a**•2CHI_3	3.32
Br	Me_2	**1b**	$CHCl_3$	**1b**	3.28
			CH_2Cl_2	**1b**•2CHI_3	3.22
Cl	Et_2	**2**	$CHCl_3$	**2**•2CHI_3	3.33
Cl	$(CH_2)_4$	**3**	$CHCl_3$	**3**•2CHI_3	2.26
Cl	$(CH_2)_5$	**4**	$CHCl_3$/hexane	**4**[a]	2.05
			$CHCl_3$	**4**•2CHI_3	3.45

[a] Previously reported[1, 2] structures.

Five bis(dialkylcyanamide) complexes *trans*-$[PtX_2(NCNR_2)_2]$ (X = Cl, R_2 = Me_2 **1a**, Et_2 **2**, $(CH_2)_4$ **3**, $(CH_2)_5$ **4**; X = Br, R_2 = Me_2 **1b**) form associates with two CHI_3 upon crystallization from complex:CHI_3 = 1:2 solutions in chloroform (**1a**•½$CHCl_3$•1½CHI_3, **2**•2CHI_3, **3**•2CHI_3 and **4**•2CHI_3) or in dichloromethane (isostructural **1a**•2CHI_3 and **1b**•2CHI_3). Three *trans*-bis(dialkylcyanamide) platinum(II) complexes were studied in this (**1b**, **Figure 11S**) or in the previous (**1a**[1] and **4**[2]) works by XRD conducted at the same (100 K) or similar (120 K) temperatures (**Table 1S**). All these data combined in **Table 2S** allowed the comparison of the bond lengths in the XRD structures.

Table 2S. The Pt–X bond lengths in CHI_3-free complexes **1a**, **1b**, and **4**, and in the CHI_3-associates.

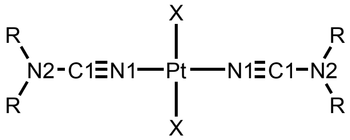

Structure	Bond	Bond Length, Å	Short Contacts
1a	**Pt1–Cl1**	**2.292(3)**	C–H•••Cl–Pt
	Pt1–N1	1.973(8)	–
	N1≡C1	1.129(14)	–
	C1–N2	1.302(14)	–
4	**Pt1–Cl1**	**2.2882(9)**	C–H•••Cl–Pt
	Pt1–N1	1.944(3)	–
	N1≡C1	1.144(4)	–
	C1–N2	1.306(4)	–
1a•½$CHCl_3$•1½CHI_3	**Pt1A–Cl1A**	**2.3023(16)**	HI_2C–I•••Cl–Pt and C–H•••Cl–Pt
	Pt1–N1	1.970(5)	–
	N1≡C1	1.135(7)	–
	C1–N2	1.297(8)	–
	Pt1–Cl1	**2.3019(12)**	HI_2C–I•••Cl–Pt and HI_2C–I•••Pt
	Pt1–N1	1.969(4)	–
	N1≡C1	1.143(6)	–
	C1–N2	1.299(6)	–
1a•2CHI_3	**Pt1–Cl1**	**2.3090(14)**	HI_2C–I•••Cl–Pt and C–H•••Cl–Pt
	Pt1–N1	1.961(5)	–
	N1≡C1	1.142(8)	–
	C1–N2	1.310(8)	–
	Pt1A–Cl1A	**2.3226(14)**	HI_2C–I•••Cl–Pt and HI_2C–I•••Pt
	Pt1–N1	1.957(5)	–
	N1≡C1	1.150(8)	–
	C1–N2	1.297(8)	–
2•2CHI_3	**Pt1–Cl1**	**2.3129(12)**	HI_2C–I•••Cl–Pt
	Pt1–N1	1.963(4)	–
	N1≡C1	1.157(6)	–
	C1–N2	1.297(6)	–
3•2CHI_3	**Pt1–Cl1**	**2.3179(7)**	HI_2C–I•••Cl–Pt
	Pt1–N1	1.965(2)	–
	N1≡C1	1.147(4)	–
	C1–N2	1.301(4)	–
4•2CHI_3	**Pt1–Cl1**	**2.3098(17)**	HI_2C–I•••Cl–Pt and HI_2C–I•••Pt
	Pt1–N1	1.960(6)	–
	N1≡C1	1.153(8)	–
	C1–N2	1.304(8)	–
1b	**Pt1–Br1**	**2.4341(6)**	C–H•••Br–Pt
	Pt1–N1	1.964(5)	–
	N1≡C1	1.140(8)	–
	C1–N2	1.304(8)	–

1b•2CHI_3	**Pt1–Br1**	**2.4494(6)**	HI_2C–I•••Br–Pt and C–H•••Br–Pt
	Pt1–N1	1.958(6)	–
	N1≡C1	1.152(9)	–
	C1–N2	1.306(9)	–
	Pt1A–Br1A	**2.4522(7)**	HI_2C–I•••Br–Pt and HI_2C–I•••Pt
	Pt1–N1	1.961(6)	–
	N1≡C1	1.145(9)	–
	C1–N2	1.312(9)	–

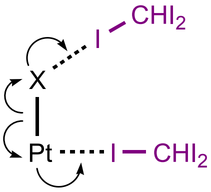

Figure 1S. The Pt–X bonds elongation due to the HI_2C–I•••X–Pt and HI_2C–I•••Pt weak interactions.

As mentioned in the main text, the elongation of the Pt–X (X = Cl, Br) bonds in the CHI_3-associates was detected when these species were compared with CHI_3-free **1a**, **1b**, and **4** (**Table 2S**). The distances Pt–Cl in **2**•2CHI_3 and **3**•2CHI_3 are also longer than in CHI_3-free complexes **1a** and **4**. Although these differences are not too large and spans the range from 0.01 to 0.03 Å, they indirectly point out (**Figure 1S**) to the presence of the HI_2C–I•••X–Pt and HI_2C–I•••Pt weak interactions (see sections **XR2** and **TH1**). It should be also mentioned that the cyanamide moieties N1≡C1–N2 and corresponding coordination bond lengths Pt1–N1 do not demonstrate any detectable differences.

XR2. General description of the CHI_3 associates of *trans*-bis(dialkylcyanamide)Pt^{II} complexes

All crystals (**1a**•½$CHCl_3$•1½CHI_3, **1a**•2CHI_3, **1b**•2CHI_3, **2**•2CHI_3, **3**•2CHI_3, and **4**•2CHI_3) are centrosymmetric, whereas in **2**•2CHI_3, **3**•2CHI_3, and **4**•2CHI_3, independent parts contain the complex lying in a special position and one CHI_3. On the contrary, two halves of complex moieties and two solvent molecules in the independent parts of **1a**•½$CHCl_3$•1½CHI_3, **1a**•2CHI_3, and **1b**•2CHI_3 were observed. Noteworthy that crystallization of a **1a**:CHI_3 mixture from chloroform led to a substitution disorder of a half of CHI_3 with $CHCl_3$ giving **1a**•½$CHCl_3$•1½CHI_3.

All crystal structures exhibit 2D-layers of the complexes surrounded by CHI_3 (**Figures 2S–3S**). In **2**•2CHI_3, **3**•2CHI_3, and **4**•2CHI_3 (**Figure 3S**, **D**, **E**, and **F**, respectively), only one crystallographically independent type of molecules of the complexes and CHI_3 was found, which form independent 2D-layers with no weak interactions between the layers. The integrity of these crystals is probably provided by dispersive interactions. The structures of **1a**•½$CHCl_3$•1½CHI_3, **1a**•2CHI_3, and **1b**•2CHI_3 (**Figure 1S**, **A**, **B** and **C**, correspondingly) are more complex as they contain two types of complexes and two types of CHI_3 molecules and also two types of 2D-layers alternate each other and linked by HB’s and I•••I XB’s. In the case of **1a**•½$CHCl_3$•1½CHI_3, one CHI_3 is partially substituted by a chloroform molecule with crystallographic occupancy ½.

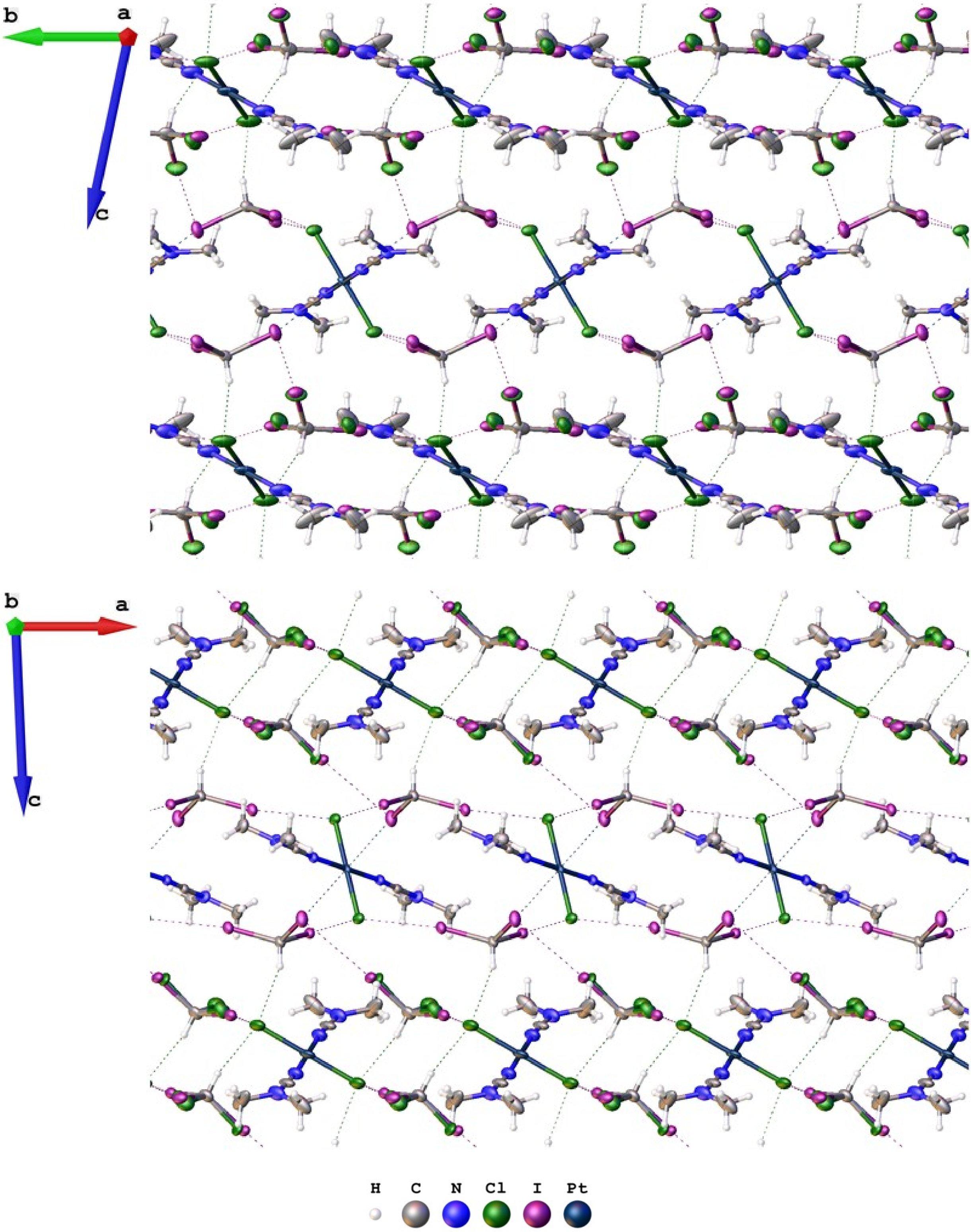

A

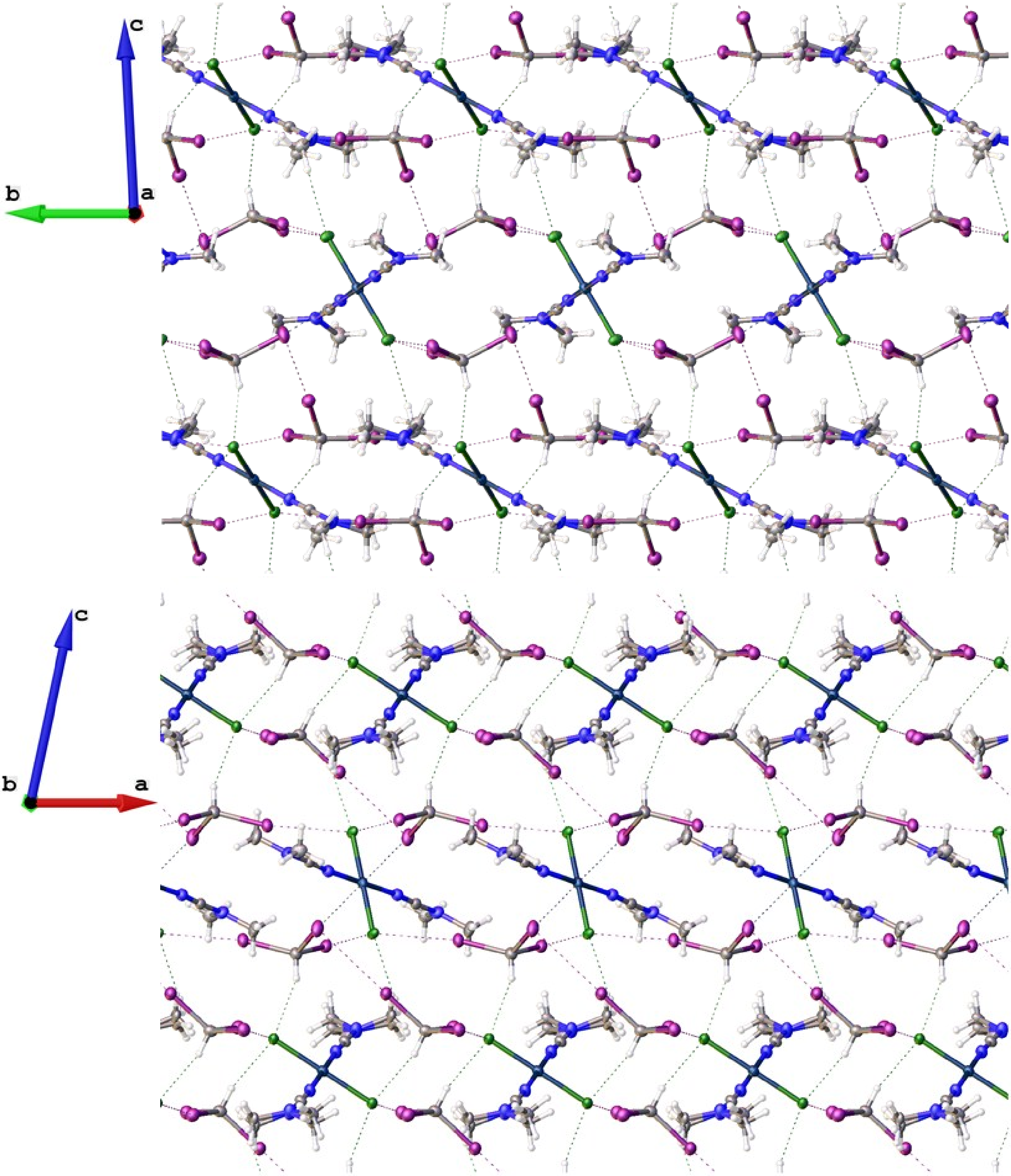

B

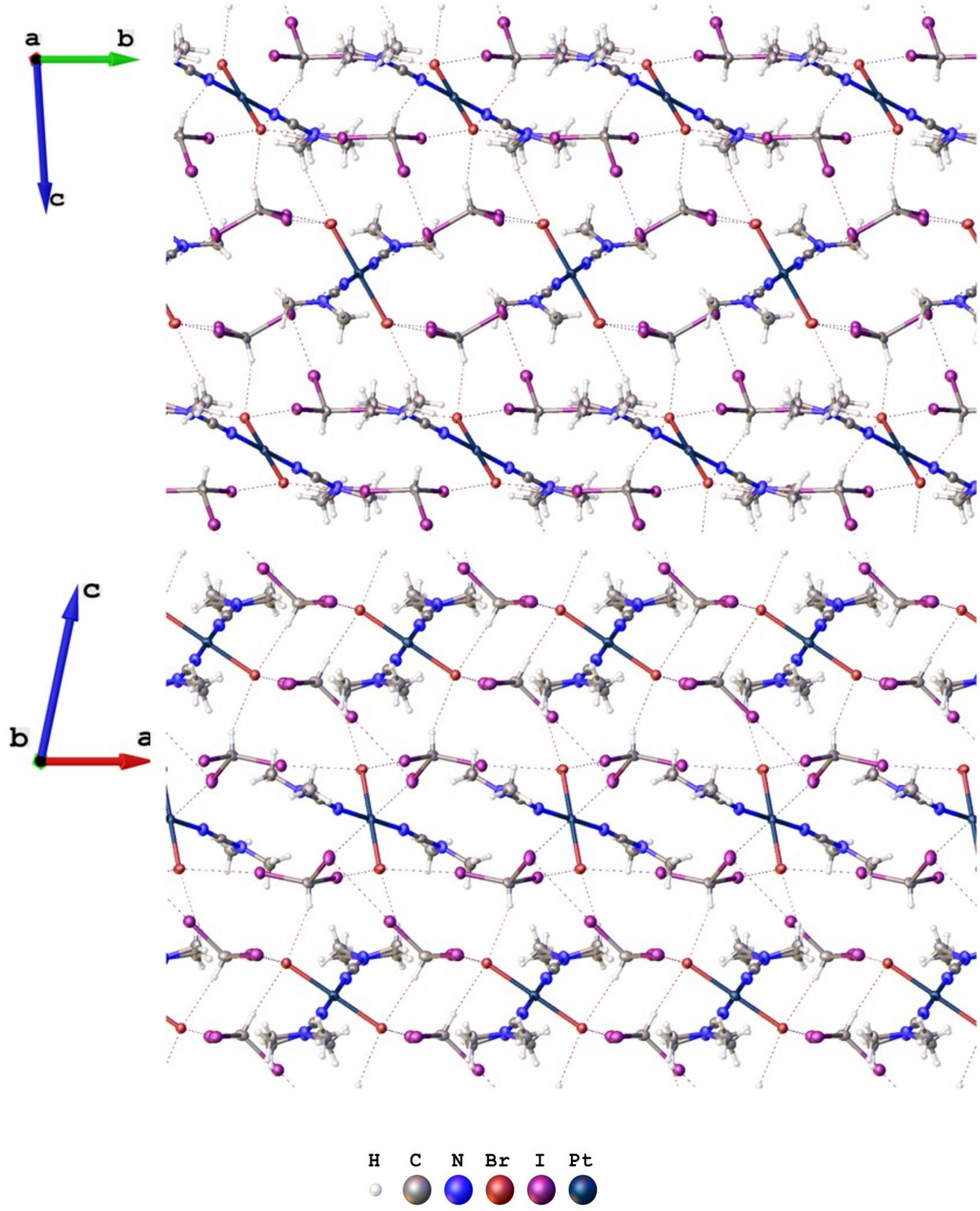

C

Figure 2S. Views along *a* and *b* axis of **1a**•½$CHCl_3$•1½CHI_3 (**A**), **1a**•2CHI_3 (**B**), and **1b**•2CHI_3 (**C**).

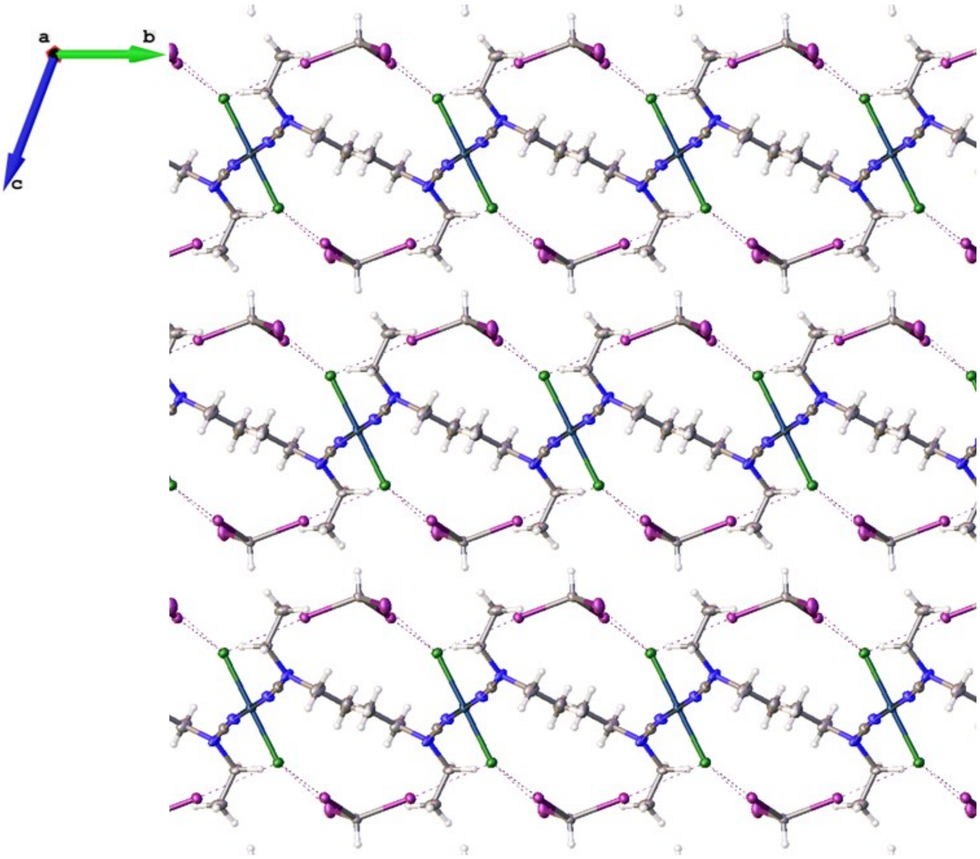

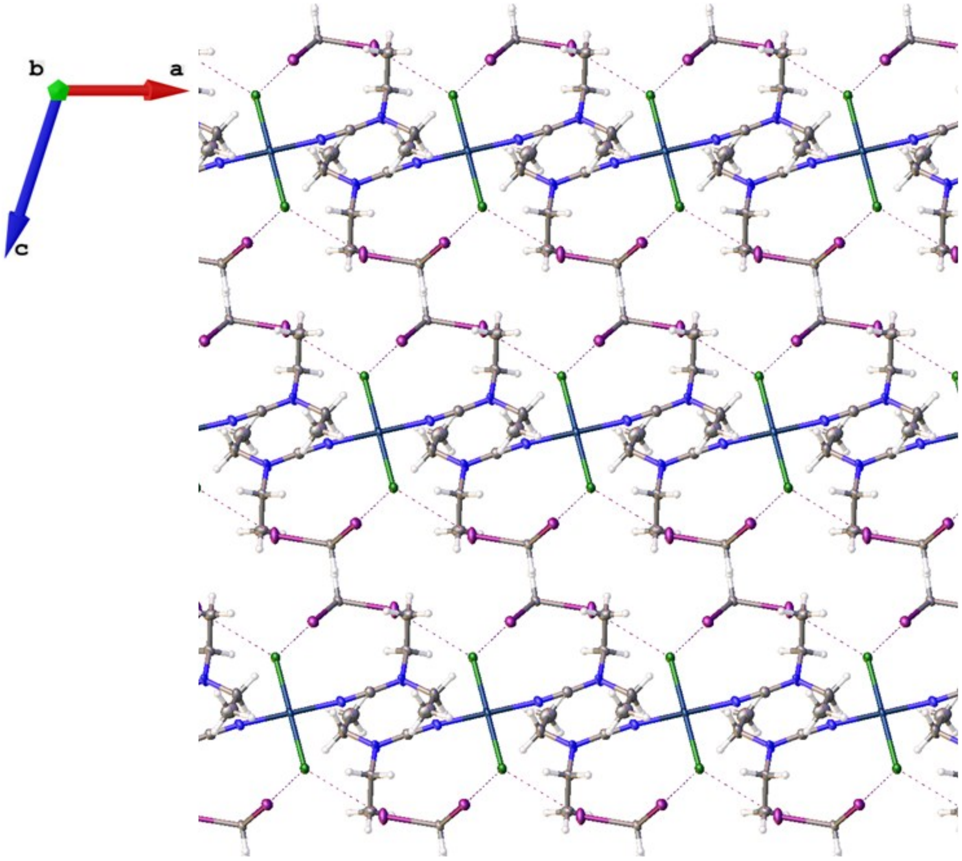

D

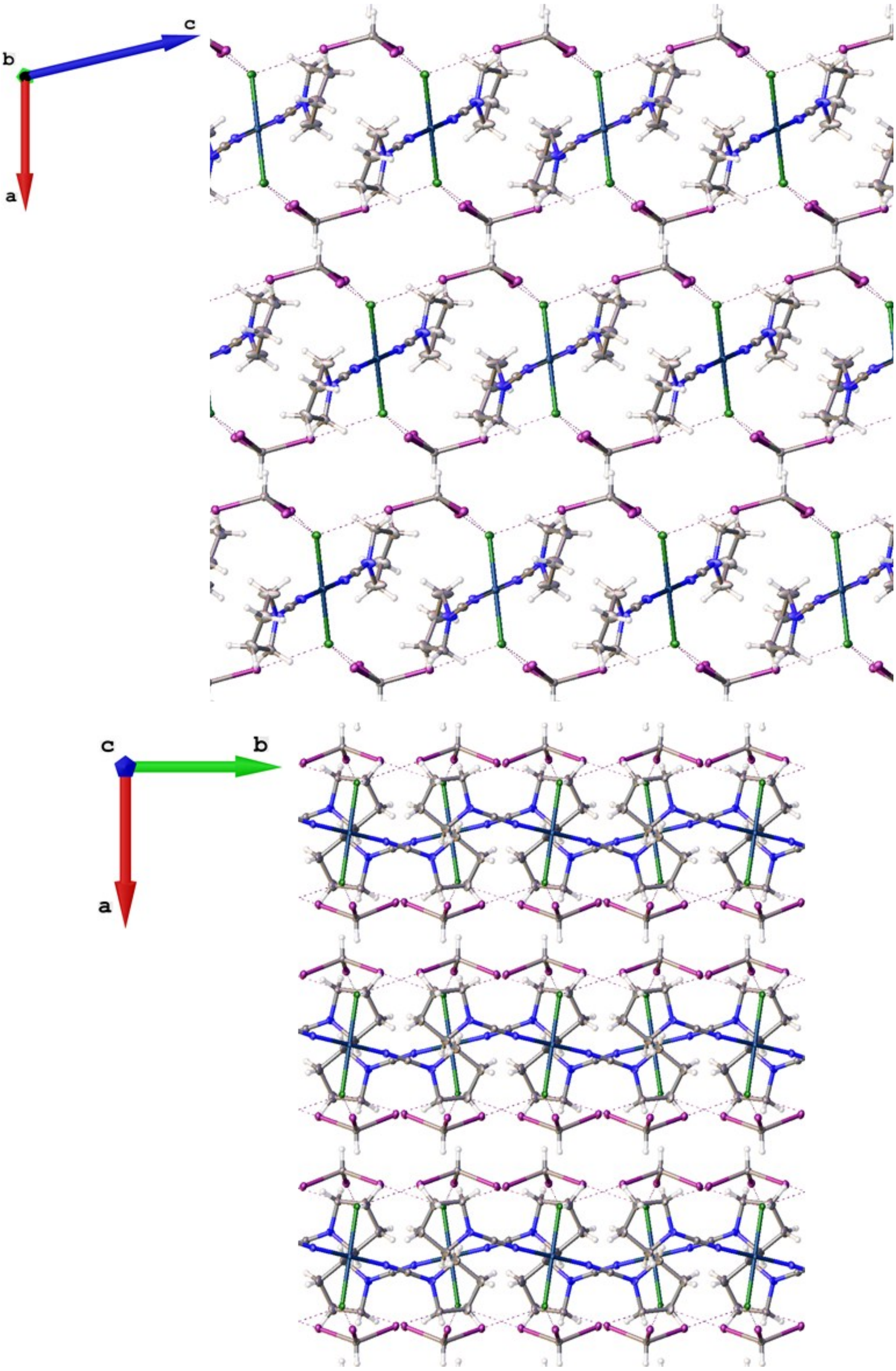

E

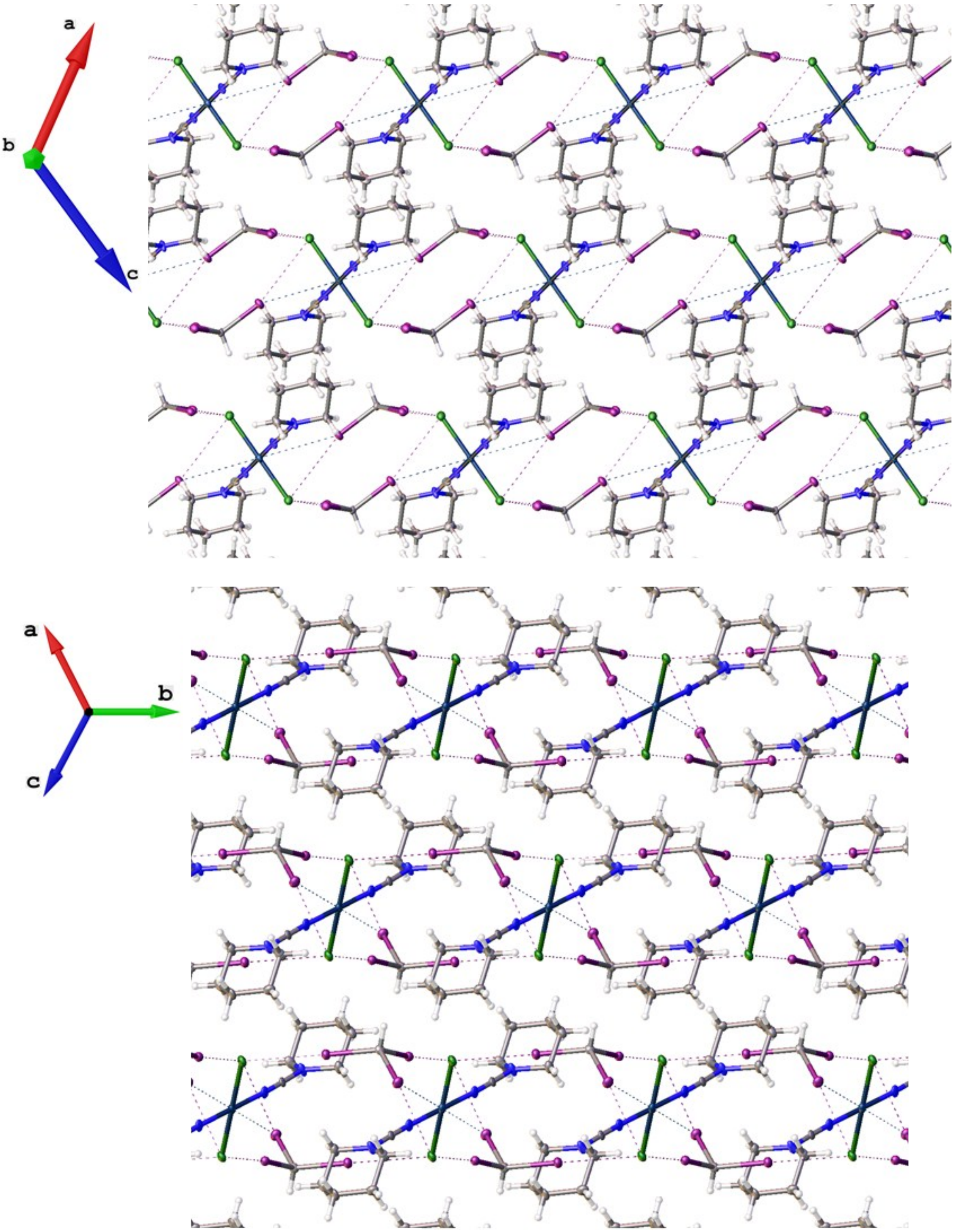

F

Figure 3S. Views of **2**•2CHI$_3$ (**D**, along *a* and *b* axis), **3**•2CHI$_3$ (**E**, along *b* and *c* axis), and **4**•2CHI$_3$ (**F**).

In the description of all short contacts in the associates, we concentrated on surroundings of each complex molecule (**Table 3S**), where molecules of CHI_3 (or $CHCl_3$ in the case of **1a**•½$CHCl_3$•1½CHI_3) formally act as second-sphere Lewis-acid species.[3] In the most cases, complexes are surrounded by six CHI_3 forming six short contacts. However, associates **1a**•½$CHCl_3$•1½CHI_3, **1a**•2CHI_3, and **1b**•2CHI_3 featuring two types of complexes and one of complex molecules is surrounded by eight CHI_3 (in the case of **1a**•½$CHCl_3$•1½CHI_3, six of them alternate with chloroform molecules; two boundary cases with only CHI_3 or only $CHCl_3$ are shown in **Table 3S**).

Table 3S. Surroundings of the complexes in the associates.

Associate	Cluster	Figure
1a·½CHCl$_3$•1½CHI$_3$	**1a**•(CHI$_3$)$_6$	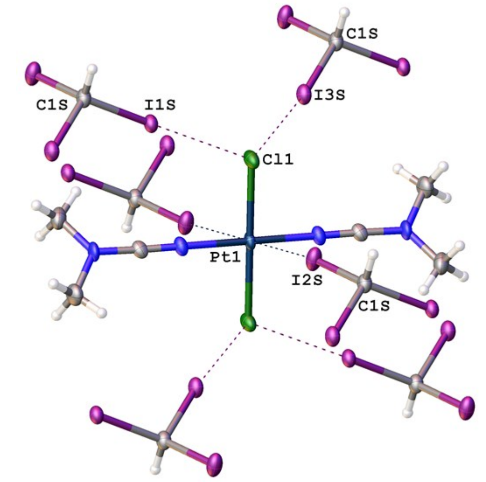
	1a•(CHI$_3$)$_8$	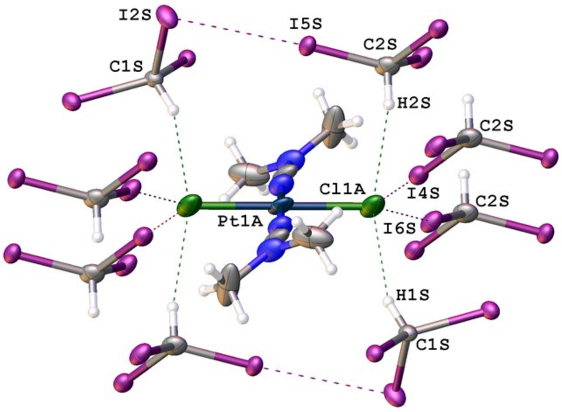
	1a•(CHI$_3$)$_2$•(CHCl$_3$)$_6$	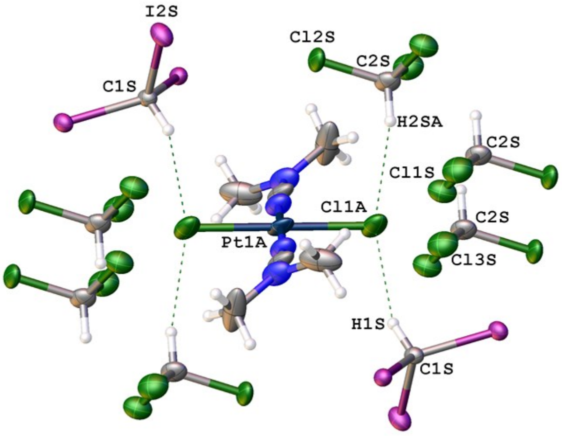

1a•2CHI$_3$	**1a**•(CHI$_3$)$_6$	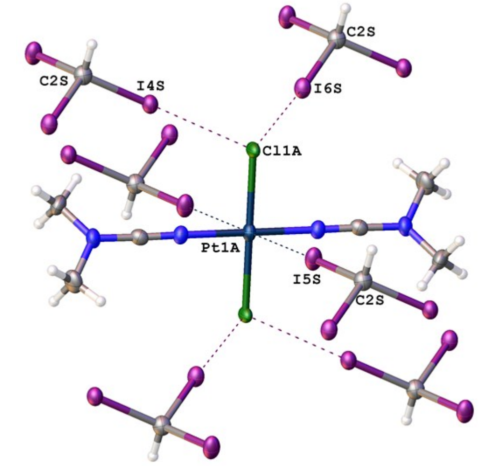
	1a•(CHI$_3$)$_8$	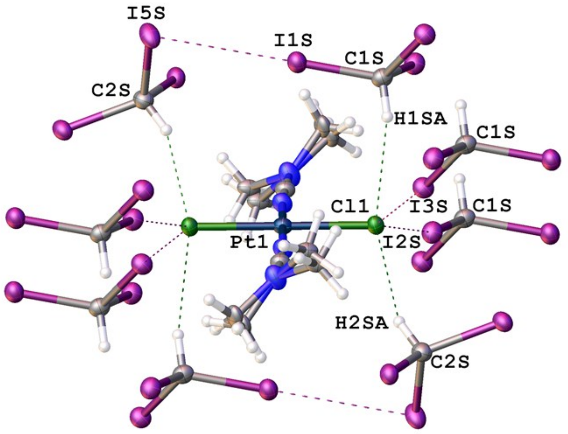
1'•2CHI$_3$	**1b**•(CHI$_3$)$_6$	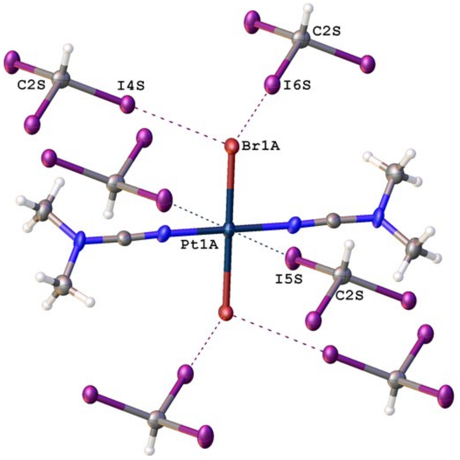
	1b•(CHI$_3$)$_8$	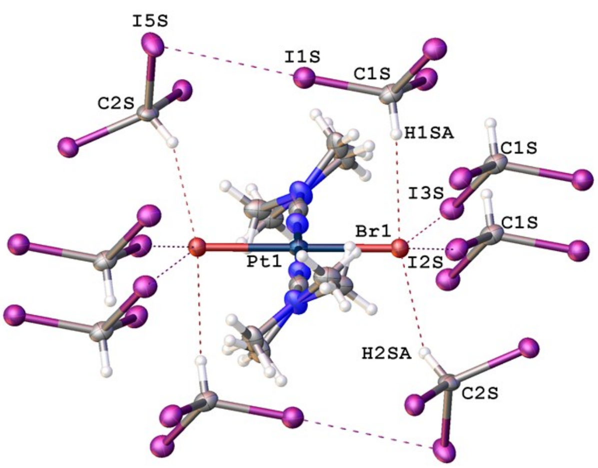

2•2CHI$_3$	**2**•(CHI$_3$)$_6$	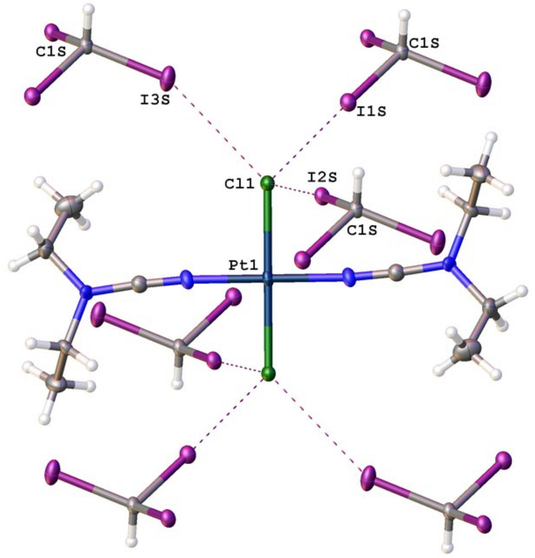
3•2CHI$_3$	**3**•(CHI$_3$)$_6$	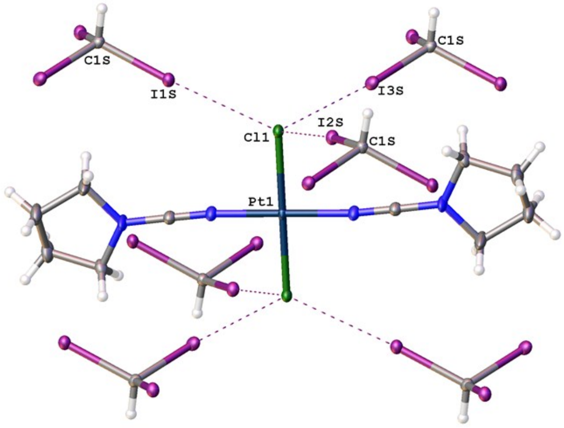
4•2CHI$_3$	**4**•(CHI$_3$)$_6$	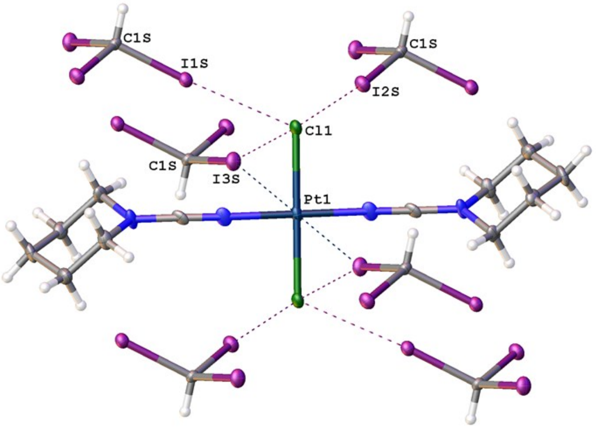

Hereinafter we describe only geometrical parameters of weak interactions. In the most cases, they are in full agreement with the IUPAC criteria for HB's[4] and XB's.[5] Moreover, the bond critical points (3, –1) were verified by theoretical calculations for the most observed contacts (see section **TH1**).

In all associates, each Pt atom lies at the inversion center. Predominantly the formation of the HI_2C–I•••X–Pt XB's was detected (**Table 4S**). However, three associates, viz. **1a**•½$CHCl_3$•1½CHI_3, **1a**•2CHI_3, and **1b**•2CHI_3, display unusual HI_2C–I•••Pt XB's (**Table 5S**), and **4**•2CHI_3 exhibit the unique bifurcated HI_2C–I•••(Cl–Pt) XB (C1S–I3S•••Cl1–Pt1 and C1S–I3S•••Pt1 in corresponding **Tables 4S** and **5S**). Apart from that, in another type of environment of complex molecules in **1a**•½$CHCl_3$•1½CHI_3, **1a**•2CHI_3, and **1b**•2CHI_3, the I_3C–H•••X–Pt and Cl_3C–H•••X–Pt HB's were found (**Table 6S**). Interestingly that two CHI_3 can form the HI_2C–I•••I–CHI_2 XB's between even each other (**Table 7S**). Noteworthy that no examples of HB's between CHI_3 and free- or metal-bound chlorides and bromides were found in the Cambridge Crystallography Database,[6] and XB's between CHI_3 were detected only in pure crystalline iodoform.[7] In **1a**•½$CHCl_3$•1½CHI_3, chloroform form only HB's with chloride ligands because the corresponding Cl1S•••Cl1A, Cl3S•••Cl1A, and Cl2S•••I2S distances are higher than the sums of Bondi's vdW radii (3.572(7) Å and 3.639(11) Å vs. $2R_{vdW}(Cl) = 3.50$ Å, and 3.893(11) Å vs. $R_{vdW}(Cl) + R_{vdW}(I) = 3.73$ Å, respectively).

In order to unambiguously reveal all bonding intermolecular interactions, the topological analysis of theoretical electron density function $\rho(\mathbf{r})$ was performed using DFT calculations of model cluster systems with experimental geometric parameters (**Table 3S**, for details see **TH1**). Within the framework of Bader's "Atoms in Molecules" (AIM) theory, the (3, –1) critical points (bond critical points, BCPs) of $\rho(\mathbf{r})$ function were found for nearly all previously mentioned contacts (H•••Cl, H•••Br, I•••Cl, I•••Br, I•••I, and I•••Pt) that reflect their attractive nature. Corresponding energies E_{int} were also determined using semi-empirical correlations between local energy densities in BCPs and interaction's strength.[8, 9] Geometric data and E_{int} values are summarized in **Tables 4S–7S**.

Table 4S. Parameters and calculated energies of HI_2C–I•••X–Pt XB’s.

Structure	C–I•••X–Pt	*d*(I•••X), Å	∠(C–I•••X),°	∠(I•••X–Pt),°	E_{int}^b	E_{int}^c
1a•½$CHCl_3$•1½CHI_3	C1S–I1S•••Cl1–Pt1	3.2833(18)	176.65(12)	113.49(5)	3.1	2.7
	C1S–I3S•••Cl1–Pt1	3.3294(13)	169.96(15)	108.53(5)	2.8	2.7
	C2S–I4S•••Cl1A–Pt1A	3.137(3)	159.7(2)	111.08(10)	–	–
	C2S–I6S•••Cl1A–Pt1A	3.185(4)	166.40(17)	118.59(10)	–	–
1a•2CHI_3	C2S–I4S•••Cl1A–Pt1A	3.322(2)	179.3(2)	114.89(6)	–	–
	C2S–I6S•••Cl1A–Pt1A	3.3778(15)	170.2(2)	107.12(6)	–	–
	C1S–I2S•••Cl1–Pt1	3.3140(19)	167.20(16)	115.28(5)	2.8	2.7
	C1S–I3S•••Cl1–Pt1	3.3309(15)	161.6(2)	110.91(6)	2.8	2.7
1b•2CHI_3	C2S–I4S•••Br1A–Pt1A	3.4004(11)	178.44(16)	113.80(3)	2.8	2.7
	C2S–I6S•••Br1A–Pt1A	3.4525(8)	170.9(2)	105.33(3)	2.5	2.2
	C1S–I2S•••Br1–Pt1	3.4189(11)	169.9(2)	114.63(2)	2.8	2.4
	C1S–I3S•••Br1–Pt1	3.4543(8)	161.7(3)	110.69(3)	2.8	2.4
2•2CHI_3	C1S–I1S•••Cl1–Pt1	3.2446(16)	177.41(15)	124.26(5)	3.1	3.0
	C1S–I2S•••Cl1–Pt1	3.2898(14)	176.92(14)	88.43(4)	3.1	3.0
	C1S–I3S•••Cl1–Pt1	3.5122(11)	155.80(15)	136.76(6)	1.9	1.9
3•2CHI_3	C1S–I1S•••Cl1–Pt1	3.2683(7)	168.57(8)	118.19(3)	3.1	3.0
	C1S–I2S•••Cl1–Pt1	3.2765(8)	174.31(8)	101.17(2)	3.1	3.0
	C1S–I3S•••Cl1–Pt1	3.2877(7)	175.51(7)	100.81(2)	3.1	2.7
4•2CHI_3	C1S–I1S•••Cl1–Pt1	3.2320(16)	175.7(2)	114.63(7)	3.5	3.0
	C1S–I2S•••Cl1–Pt1	3.327(2)	175.44(14)	106.18(7)	2.8	2.7
	C1S–I3S•••Cl1–Pt1	3.6974(19)	163.4(2)	72.03(5)	1.3	1.4
	Comparison[a]	*3.73 (I•••Cl)* *3.83 (I•••Br)*	*180*	*90*		

[a] Comparison with the sum of Bondi’s vdW radii and with the typical halogen bond angle.

[b] $E_{int} = -V(\mathbf{r})/2$[8]

[c] $E_{int} = 0.429G(\mathbf{r})$[9]

Table 5S. Parameters and calculated energies of HI_2C–I•••Pt XB’s.

Structure	C–I•••Pt	*d*(I•••Pt), Å	∠(C–I•••Pt),°	E_{int}^b	E_{int}^c
1a•½$CHCl_3$•1½CHI_3	C1S–I2S•••Pt1	3.4276(5)	164.84(17)	2.8	2.4
1a•2CHI_3	C2S–I5S•••Pt1A	3.4389(5)	169.8(3)	–	–
1b•2CHI_3	C2S–I5S•••Pt1A	3.4023(5)	172.7(2)	3.1	2.7
4•2CHI_3	C1S–I3S•••Pt1	3.7060(7)	158.4(2)	1.6	1.6
	Comparison[a]	*3.73*	*180*		

Comparison with the sum of Bondi’s vdW radii and with the typical halogen bond angle.

[b] $E_{int} = -V(\mathbf{r})/2$[8]

[c] $E_{int} = 0.429G(\mathbf{r})$[9]

Table 6S. Parameters and calculated energies of $I_3C–H\bullet\bullet\bullet X–Pt$ HB's.

Structure	C–H•••X–Pt	*d*(X•••H), Å	*d*(X•••C), Å	∠(C–H•••X),°	*E_{int}*[b]	*E_{int}*[c]
1a•½$CHCl_3$•1½CHI_3	C1S–H1S•••Cl1A	2.5257(15)	3.455(5)	158.2(3)	–	–
	C2S–H2S•••Cl1A	2.6066(16)	3.543(6)	160.1(3)	–	–
	C2S–H2AS•••Cl1A	2.6048(16)	3.543(6)	160.5(3)	–	–
1a•2CHI_3	C2S–H2AS•••Cl1	2.5524(16)	3.496(8)	157.0(4)	2.5	2.4
	C1S–H1AS•••Cl1	2.7560(14)	3.684(6)	154.5(3)	1.6	1.6
1b•2CHI_3	C2S–H2AS•••Br1	2.6813(7)	3.602(8)	153.3(4)	2.5	2.2
	C1S–H1AS•••Br1	2.8576(6)	3.785(8)	154.4(5)	1.6	1.6
	Comparison[a]	*2.95 (Cl•••H)* *3.05 (Br•••H)*	*3.45 (Cl•••C)* *3.55 (Br•••C)*	*120*		

Comparison with the sum of Bondi's vdW radii and with the minimal hydrogen bond angle.

[b] $E_{int} = –V(\mathbf{r})/2$[8]

[c] $E_{int} = 0.429G(\mathbf{r})$[9]

Table 7S. Parameters and calculated energies of $HI_2C–I\bullet\bullet\bullet I–CHI_2$ XB's.

Structure	C–I•••I–C	*d*(I•••I), Å	∠(C–I•••I),°	∠(I•••I–C),°	*E_{int}*[b]	*E_{int}*[c]
1a•½$CHCl_3$•1½CHI_3	C2S–I5S•••I2S–C1S	3.621(3)	177.14(19)	87.26(13)	–	–
1a•2CHI_3	C1S–I1S•••I5S–C2S	3.7186(6)	177.6(2)	86.12(17)	2.2	2.2
1b•2CHI_3	C1S–I1S•••I5S–C2S	3.7601(7)	176.5(3)	84.18(18)	1.9	1.9
	Comparison[a]	*3.96*	*180*	*90*		

[a]Comparison with the sum of Bondi's vdW radii and with the typical halogen bond angles.

[b] $E_{int} = –V(\mathbf{r})/2$[8]

[c] $E_{int} = 0.429G(\mathbf{r})$[9]

XR3. Variable temperature XRD study of 4•2CHI_3

Insofar as the observed bifurcated $HI_2C–I\bullet\bullet\bullet\eta^2_{(Pt–Cl)}$ XB's in **4**•2CHI_3 is unique, we decided to obtain more information on this unusual weak interaction. For one single-crystal of **4**•2CHI_3 we collected five XRD datasets in the range of 100–300 K with a 50 K step. All corresponding geometry data as well as E_{int} values are given in **Table 8S**.

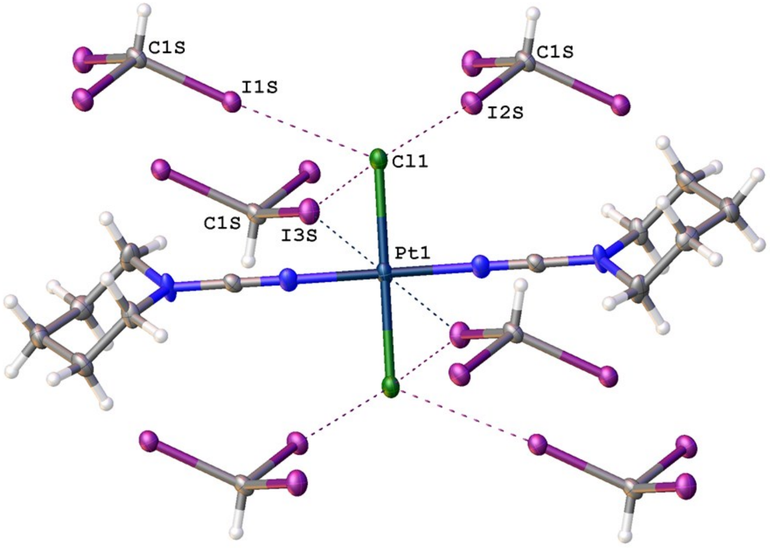

100 K

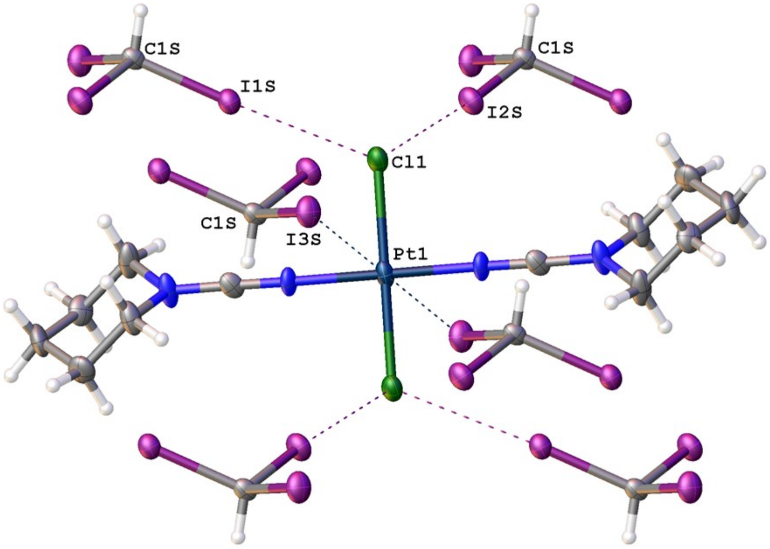

150 K

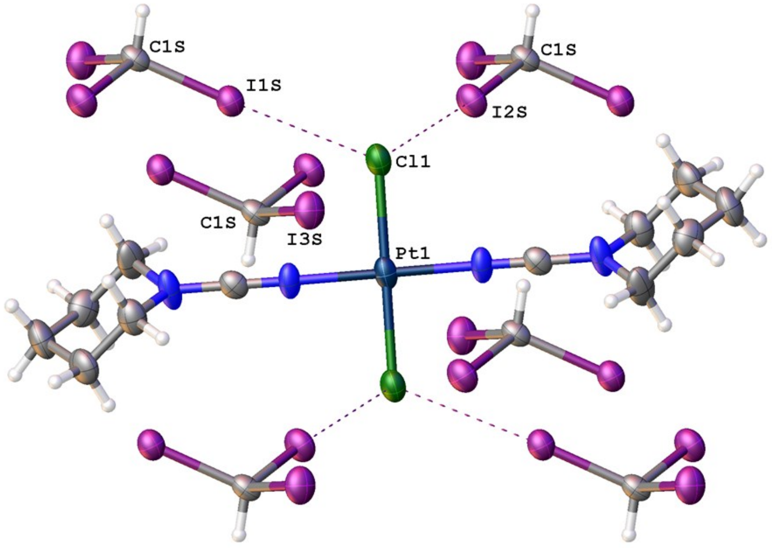

200 K

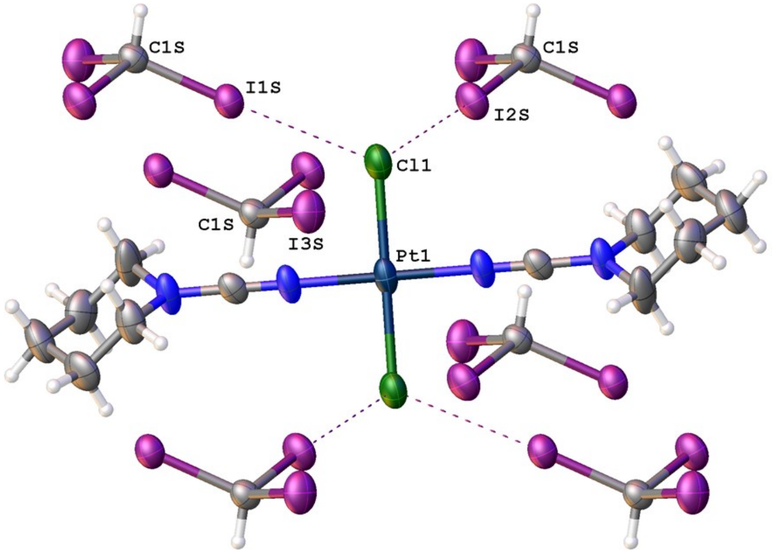

250 K

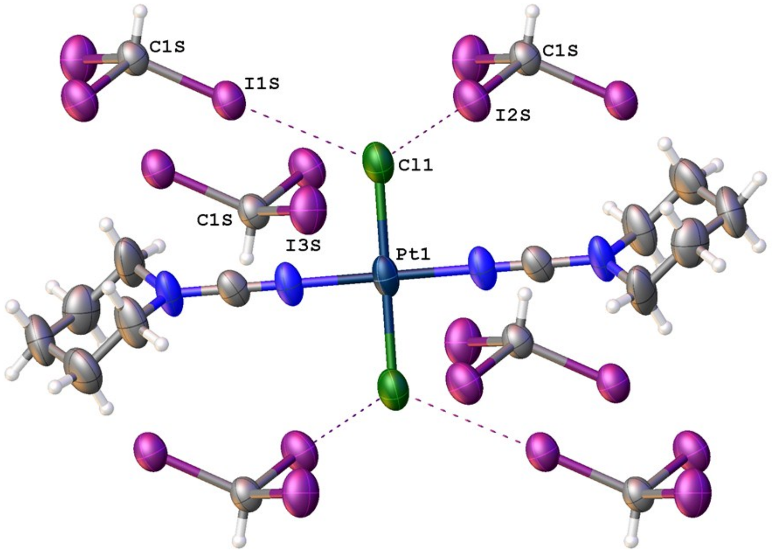

300 K

Figure 4S. View of clusters **4**•(CHI$_3$)$_6$ in **4**•2CHI$_3$ at each temperature, which was used for DFT calculations. Thermal ellipsoids are shown with the 50% probability. Contacts less than corresponding sums of Bondi's vdW radii are given in dotted lines.

Table 8S. Parameters and calculated energies of XB's in **4**•2CHI$_3$ at different temperatures.

XB	T, K	*d*(I•••X), Å	∠(C–I•••X), °	∠(I•••Cl–Pt), °	E_{int}^{c}	E_{int}^{d}
C1S–I1S•••Cl1–Pt1	100	3.2344(15)	175.4(2)	114.67(6)	3.5	3.0
	150	3.2425(17)	175.5(2)	115.11(7)	3.5	3.0
	200	3.2575(17)	176.0(3)	115.60(7)	3.1	3.0
	250	3.2708(17)	176.2(2)	116.16(7)	3.1	3.0
	300	3.2853(18)	176.6(2)	116.71(7)	3.1	2.7
C1S–I2S•••Cl1–Pt1	100	3.3337(19)	175.41(16)	105.87(7)	2.8	2.7
	150	3.342(2)	175.76(15)	105.73(7)	2.5	2.4
	200	3.352(2)	175.86(16)	105.73(7)	2.5	2.4
	250	3.365(2)	175.96(14)	105.58(7)	2.5	2.4
	300	3.365(2)	176.00(13)	105.77(7)	2.5	2.4
C1S–I3S•••Cl1–Pt1	100	3.7138(19)	163.4(2)	71.84(5)	1.3	1.4
	150	3.734(2)[b]	163.3(2)	71.77(5)	1.3	1.4
	200	3.755(2)	163.5(2)	71.91(5)	1.3	1.4
	250	3.780(2)	163.7(2)	72.00(5)	1.0	1.1
	300	3.797(2)	163.9(2)	72.28(5)	–	–
C1S–I3S•••Pt1	100	3.7157(5)	158.5(2)		1.6	1.6
	150	3.7283(7)	158.7(2)		1.6	1.4
	200	3.7495(6)	158.2(2)		1.3	1.4
	250	3.7738(6)	158.0(2)		1.3	1.4
	300	3.7962(7)	158.0(2)		1.3	1.4
	Comparison[a]	*3.73 (Cl•••I)* *3.73 (Pt•••I)*	*180*	*90*		

[a]Comparison with the sum of Bondi's vdW radii and with the typical halogen bond angles.

[b]Values of lengths which are not fulfilled the IUPAC criterion (less that sums vdW radii) are given in red.

[c] $E_{int} = –V(\mathbf{r})/2$[8]

[d] $E_{int} = 0.429G(\mathbf{r})$[9]

Accordingly to the vdW IUPAC criterion,[5] the C1S–I3S•••Cl1–Pt1 and C1S–I3S•••Pt1 XB's elongates and become larger than the sum of Bondi's vdW radii at 150 and 200 K, correspondingly. However, our DFT calculations followed by AIM analysis (for details see **TH2**) indicated that even at 250 K both bond critical points (3, –1) for the contacts between the I and Pt and I and Cl atoms were preserved and the estimated energies E_{int} for both contacts are around 1 kcal/mol. At 300 K, bond critical point for the I3S•••Cl1 weak interaction was not found and it means that only the C1S–I3S•••Pt1 XB exists at 300 K, whereas the bifurcated C1S–I3S•••(Cl1–Pt1) XB can be identified only at temperatures below 250 K (**Figure 5S**). The reversibility of thermal transformations was confirmed by three consecutive XRD experiments for the same single-crystal at 100 K, at 300 K, and again at 100 K, and low temperature experiments give quite similar values for all contacts (**Table 9S**).

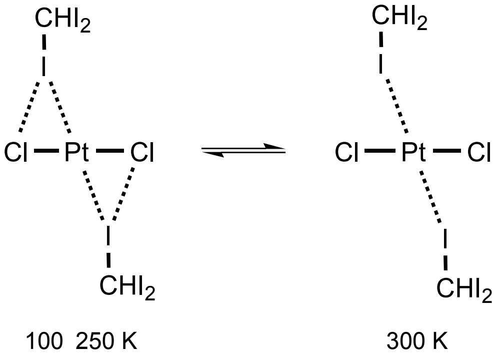

Figure 5S. Thermally induced reversible $HI_2C–I\cdots\eta^2_{(Pt–Cl)} \rightleftarrows HI_2C–I\cdots\eta^1_{(Pt)}$ transformation.

Table 9S. Interatomic distances for all short contacts in three XRD experiments at 100 K, at 300 K, and again at 100 K for the same **4**•2CHI_3 single-crystal.

Contact	100 K (first exp.)	300 K	100 K (second exp.)
C1S–I1S•••Cl1–Pt1	3.2415(16)	3.294(3)	3.2336(16)
C1S–I2S•••Cl1–Pt1	3.344(2)	3.370(3)	3.336(2)
C1S–I3S•••Cl1–Pt1	3.737(2)	3.820(3)	3.7262(19)
C1S–I3S•••Pt1	3.7222(8)	3.7982(9)	3.7133(7)

PART 2. THEORETICAL CALCULATIONS

TH1. Theoretical considerations of non-covalent interactions in the associates

Inspection of the crystallographic data indicates the presence of XB in all studied crystals. In order to clarify the situation and quantitatively estimate the energies of these non-covalent interactions in solid state, we carried out detailed theoretical study including DFT calculations and AIM analysis for cluster systems **1a**•$(CHI_3)_6$, **1a**•$(CHI_3)_8$, **1b**•$(CHI_3)_6$, **1b**•$(CHI_3)_8$, **2**•$(CHI_3)_6$, **3**•$(CHI_3)_6$, and **4**•$(CHI_3)_6$ that modelling **1a**•½$CHCl_3$•1½CHI_3, **1a**•2CHI_3, **1b**•2CHI_3, **2**•2CHI_3, **3**•2CHI_3, and **4**•2CHI_3, respectively (section **XR2**, **Table 3S**). The results are summarized in **Table 10S**. For all fixed bond critical points (BCPs) (3, –1) such parameters as electron density (low magnitude), Laplacian (positive values), and energy density (zero or very close to zero) are typical for non-covalent interactions. The energies of these weak interactions have been defined according to the procedures proposed by Espinosa et al.[8] and Vener et al.[9] The contour line diagrams of the Laplacian distribution $\nabla^2\rho(\mathbf{r})$, bond paths and selected zero-flux surfaces for some fragments in the model systems are shown in **Figure 6S**.

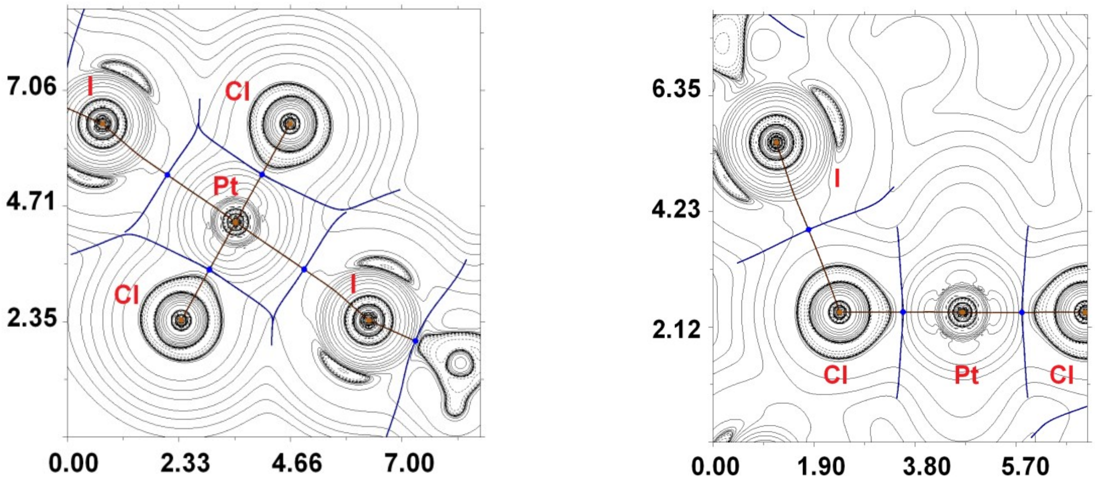

A

B

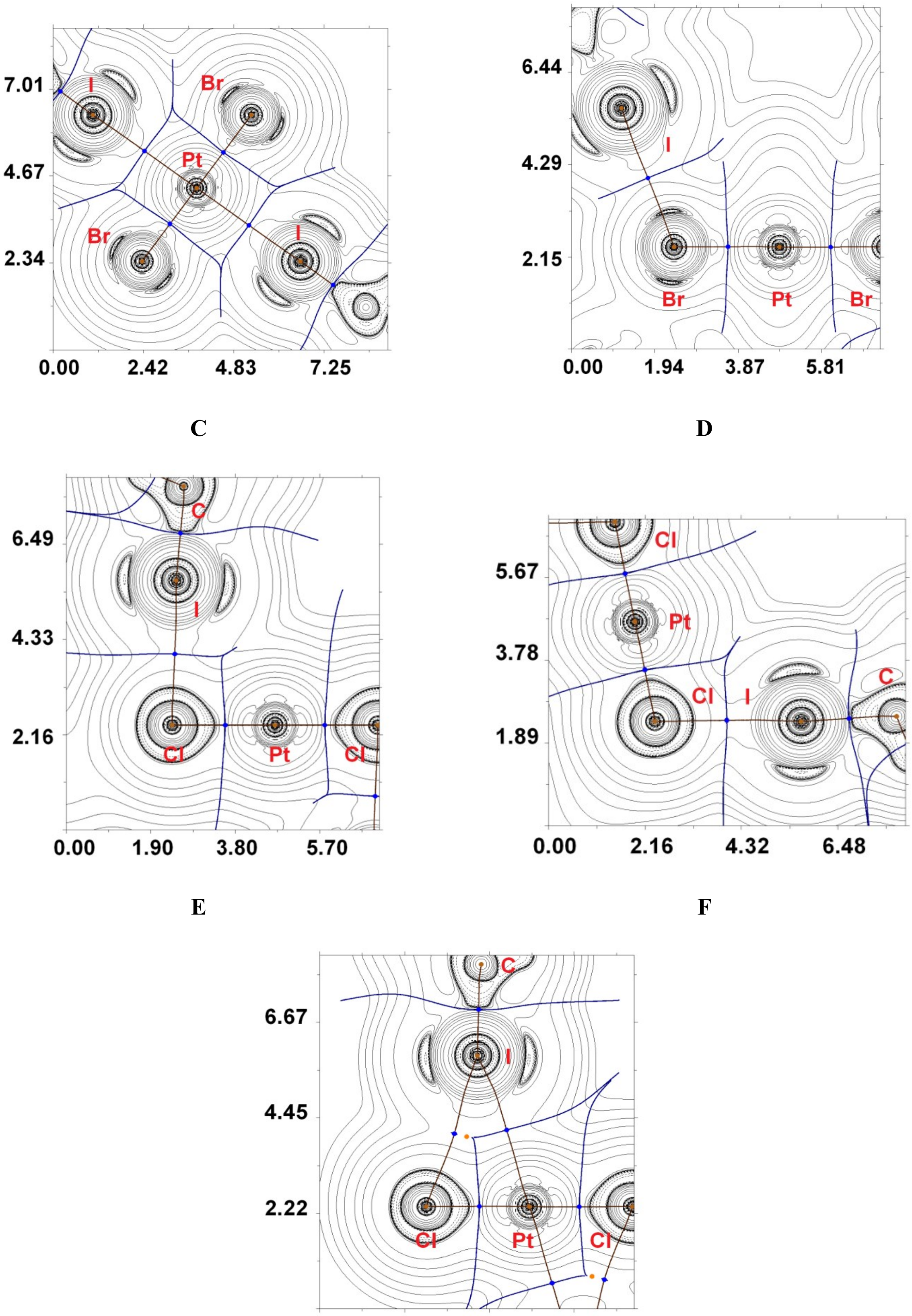

C **D**

E **F**

G

Figure 6S. Contour line diagrams of the Laplacian distribution $\nabla^2\rho(\mathbf{r})$, bond paths and selected zero-flux surfaces in four the model systems. Bond critical points (3, –1) are shown in blue, nuclear critical points (3, –3) – in pale brown, ring critical points (3, +1) – in orange, length unit – Å.

Table 10S. Values of the density of all electrons – ρ(**r**), Laplacian of electron density – ∇^2ρ(**r**), energy density – H_b, potential energy density – V(**r**), and Lagrangian kinetic energy – G(**r**) (Hartree) at the bond critical points (3, –1), corresponding to the I•••Cl, I•••Br, I•••I, H•••Cl, H•••Br, and I•••Pt weak interactions in model systems **1a**•$(CHI_3)_6$, **1b**•$(CHI_3)_6$, **2**•$(CHI_3)_6$, **3**•$(CHI_3)_6$, and **4**•$(CHI_3)_6$, and energies of these non-covalent interactions E_{int} (kcal/mol) defined by two methods.

Cluster	Contact	ρ(**r**)	∇^2ρ(**r**)	H_b	V(r)	G(r)	E_{int}[c]	E_{int}[d]
1a•$(CHI_3)_6$[a]	C1S–I1S•••Cl1–Pt1	0.015	0.045	0.001	-0.010	0.010	3.1	2.7
	C1S–I3S•••Cl1–Pt1	0.014	0.042	0.001	-0.009	0.010	2.8	2.7
	C1S–I2S•••Pt1	0.016	0.037	0.000	-0.009	0.009	2.8	2.4
1a•$(CHI_3)_8$[b]	C1S–I2S•••Cl1–Pt1	0.014	0.043	0.001	-0.009	0.010	2.8	2.7
	C1S–I3S•••Cl1–Pt1	0.014	0.044	0.001	-0.009	0.010	2.8	2.7
	C2S–H2AS•••Cl1	0.013	0.040	0.001	-0.008	0.009	2.5	2.4
	C1S–H1AS•••Cl1	0.009	0.028	0.001	-0.005	0.006	1.6	1.6
	C1S–I1S•••I5S–C2S	0.011	0.034	0.001	-0.007	0.008	2.2	2.2
1b•$(CHI_3)_6$	C2S–I4S•••Br1A–Pt1A	0.015	0.037	0.000	-0.009	0.009	2.8	2.4
	C2S–I6S•••Br1A–Pt1A	0.014	0.034	0.000	-0.008	0.008	2.5	2.2
	C2S–I5S•••Pt1A	0.017	0.038	0.000	-0.010	0.010	3.1	2.7
1b•$(CHI_3)_8$	C1S–I2S•••Br1–Pt1	0.014	0.036	0.000	-0.009	0.009	2.8	2.4
	C1S–I3S•••Br1–Pt1	0.014	0.036	0.000	-0.009	0.009	2.8	2.4
	C2S–H2AS•••Br1	0.013	0.032	0.000	-0.008	0.008	2.5	2.2
	C1S–H1AS•••Br1	0.009	0.024	0.000	-0.005	0.006	1.6	1.6
	C1S–I1S•••I5S–C2S	0.010	0.032	0.001	-0.006	0.007	1.9	1.9
2•$(CHI_3)_6$	C1S–I1S•••Cl1–Pt1	0.016	0.048	0.001	-0.010	0.011	3.1	3.0
	C1S–I2S•••Cl1–Pt1	0.015	0.045	0.001	-0.010	0.011	3.1	3.0
	C1S–I3S•••Cl1–Pt1	0.010	0.033	0.001	-0.006	0.007	1.9	1.9
3•$(CHI_3)_6$	C1S–I1S•••Cl1–Pt1	0.015	0.046	0.001	-0.010	0.011	3.1	3.0
	C1S–I2S•••Cl1–Pt1	0.015	0.046	0.001	-0.010	0.011	3.1	3.0
	C1S–I3S•••Cl1–Pt1	0.015	0.045	0.001	-0.010	0.010	3.1	2.7
4•$(CHI_3)_6$	C1S–I1S•••Cl1–Pt1	0.016	0.049	0.001	-0.011	0.011	3.5	3.0
	C1S–I2S•••Cl1–Pt1	0.014	0.042	0.001	-0.009	0.010	2.8	2.7
	C1S–I3S•••Cl1–Pt1	0.008	0.025	0.001	-0.004	0.005	1.3	1.4
	C1S–I3S•••Pt1	0.010	0.026	0.001	-0.005	0.006	1.6	1.6

[a] Calculations for the cluster **1a**•$(CHI_3)_6$ were performed on coordinates only from **1a**•½$CHCl_3$•1½CHI_3, because corresponding cluster from **1a**•2CHI_3 has the similar geometric parameters.

[b] Calculations for the cluster **1a**•$(CHI_3)_8$ were performed on coordinates from **1a**•2CHI_3, because corresponding fragment from **1a**•½$CHCl_3$•1½CHI_3 contains the $CHCl_3$/CHI_3 occupancy disorder.

[c] E_{int} = –V(**r**)/2[8]

[d] E_{int} = 0.429G(**r**)[9]

Results of the AIM analysis for **1a**•$(CHI_3)_6$ and **1b**•$(CHI_3)_6$ model systems (**Figure 6S**, **A** and **C**) confirms the presence of four "normal" I•••X XB's (E_{int} = 2.7–3.1 kcal/mol for I•••Cl and E_{int} = 2.2–2.8 kcal/mol) and two I•••Pt XB's (E_{int} = 2.4–2.8 kcal/mol and E_{int} = 2.7–3.1 kcal/mol, respectively). Location of "lone pairs" of iodine atoms also confirms that Pt atoms behave as XB acceptors.

In the cases of **1a**•$(CHI_3)_8$ and **1b**•$(CHI_3)_8$ (**Figure 6S**, **B** and **D**), we located hydrogen bonds H•••X (X = Cl, E_{int} = 2.2–2.5 kcal/mol; X = Br, E_{int} = 1.6–2.5 kcal/mol), four halogen bonds I•••X (X = Cl, E_{int} = 2.7–2.8 kcal/mol, X = Br, E_{int} = 2.4–2.8 kcal/mol), and two I•••I XB's (E_{int} = 2.2 and 1.9 kcal/mol).

For the **2**•$(CHI_3)_6$ and **3**•$(CHI_3)_6$ (**Figure 6S**, **E** and **F**, respectively) all six expected BCPs (3, –1) for the I•••Cl halogen bonding have been fixed. The estimated energies for these contacts E_{int} are in the range of 1.9–3.1 kcal/mol; no bond critical points (3, –1) between Pt and I were found in both cases.

Finally, for **4**•$(CHI_3)_6$ (**Figure 6S**, **G**) we found four "normal" I•••Cl halogen bonds (E_{int} = 2.7–3.5 kcal/mol). In addition, in this system CHI_3 forms the I•••Pt (E_{int} = 1.6 kcal/mol) and the I•••Cl (E_{int} = 1.3–1.4 kcal/mol) halogen bonding along with the Pt and Cl atoms (this phenomenon has been proven by the fixation of appropriate BCPs (3, –1) and ring critical point (3, +1) for the 3-membered cycle $(I^a\cdots Cl{-}Pt^b)^{a\cdots b}$. The location of iodine "lone pairs" also confirms that both Pt and Cl should be considered as XB acceptors.

The estimated binding energies for I•••Cl contacts are inversely proportional to their lengths; detected correlations are presented on **Figure 7S**.

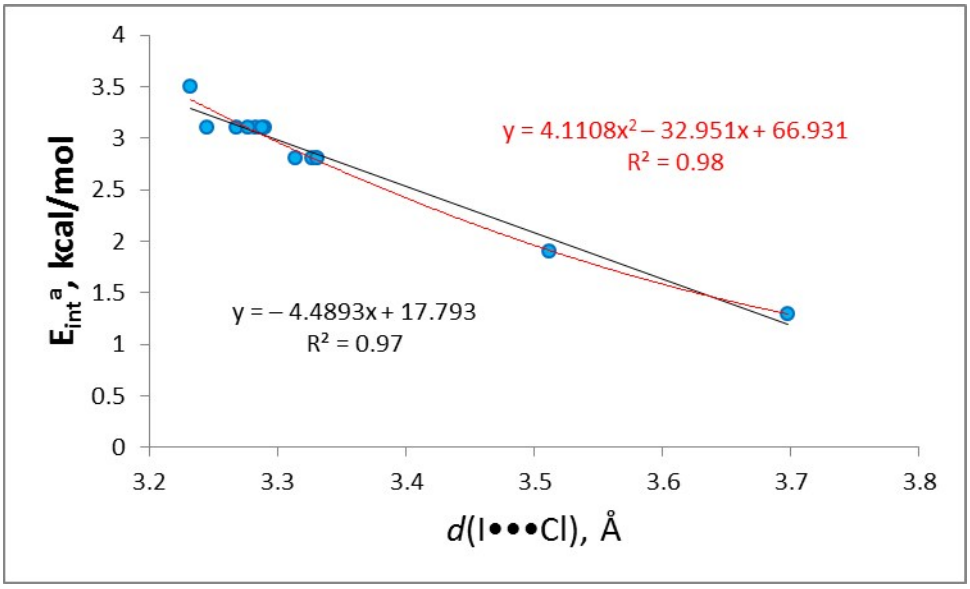

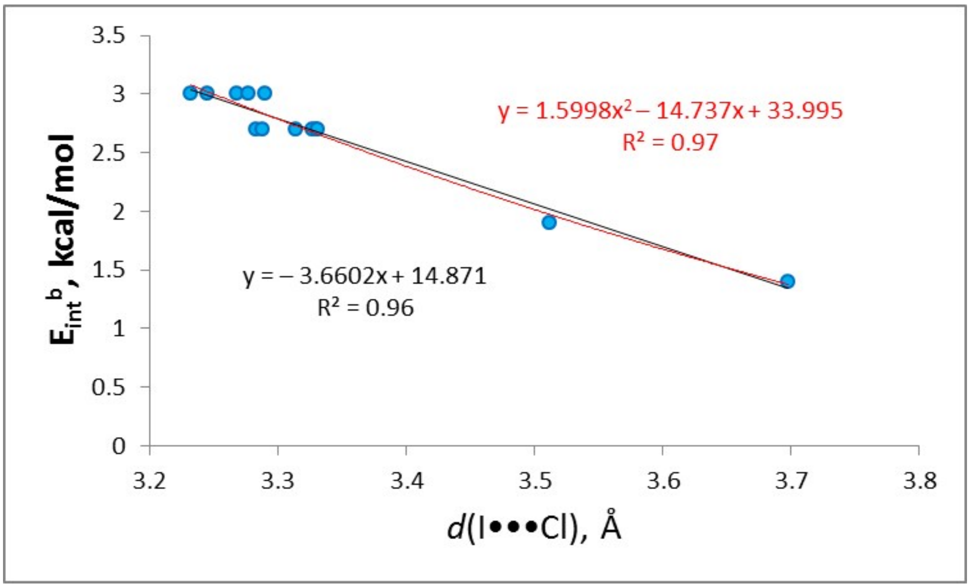

Figure 7S. The correlations between I•••Cl distances *l* (Å) in the model systems and energies of these non-covalent interactions E_{int}^{a} and E_{int}^{b} (kcal/mol) defined by two approaches.[8, 9]

TH2. Thermally induced HI_2C–I•••η^2(Pt–Cl) → HI_2C–I•••$\eta^1_{(Pt)}$ transformation: a theoretical study

As mentioned in **TH1**, for **4**•2CHI_3 we performed five XRD experiments on the same single-crystal at five temperatures ranged from 100 to 300 K. In each case, the coordinates of cluster **4**•$(CHI_3)_6$ were applied for further DFT calculations followed by AIM analysis. The main results of this study are shown at **Figure 8S** and compiled in **Table 11S**.

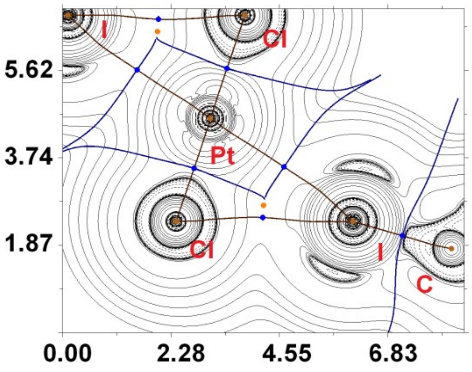

100 K

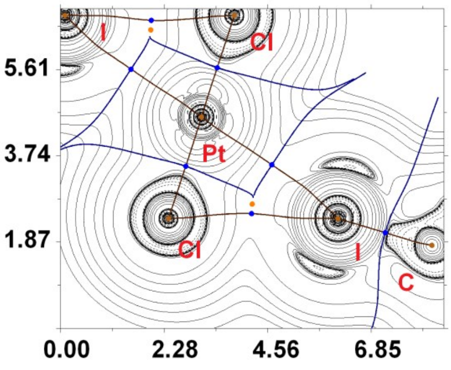

150 K

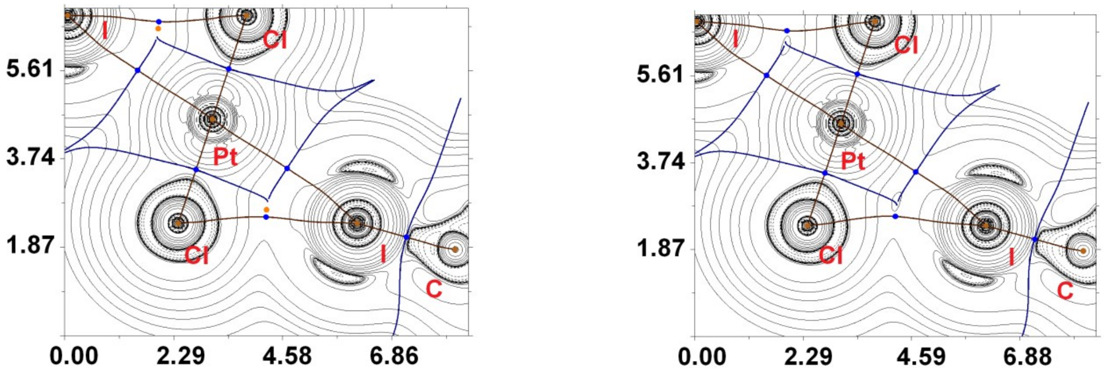

200 K **250 K**

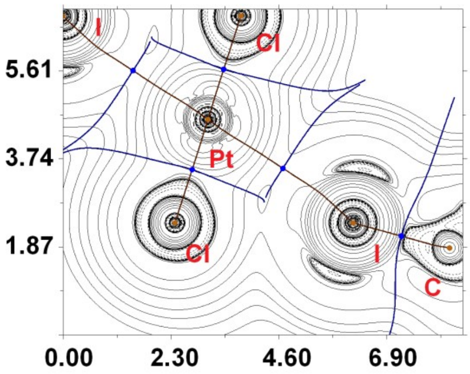

300 K

Figure 8S. Contour line diagrams of the Laplacian distribution $\nabla^2\rho(\mathbf{r})$, bond paths and selected zero-flux surfaces in five model clusters of **4**•$(CHI_3)_6$ at different temperatures. Bond critical points (3, –1) are shown in blue, nuclear critical points (3, –3) – in pale brown, ring critical points (3, +1) – in orange, length unit – Å.

Table 11S. Values of the density of all electrons – $\rho(\mathbf{r})$, Laplacian of electron density – $\nabla^2\rho(\mathbf{r})$, energy density – H_b, potential energy density – $V(\mathbf{r})$, and Lagrangian kinetic energy – $G(\mathbf{r})$ (Hartree) at the bond critical points (3, –1), corresponding to the I•••Cl and I•••Pt weak interactions in model systems **4**•$(CHI_3)_6$ at each temperature, and energies of these non-covalent interactions E_{int} (kcal/mol), defined by two methods.

Contact	T, K	$\rho(\mathbf{r})$	$\nabla^2\rho(\mathbf{r})$	H_b	V(r)	G(r)	E_{int}[a]	E_{int}[b]
C1S–I1S•••Cl1–Pt1	100	0.014	0.042	0.001	-0.009	0.010	2.8	2.7
	150	0.014	0.041	0.001	-0.008	0.009	2.5	2.4
	200	0.013	0.041	0.001	-0.008	0.009	2.5	2.4
	250	0.013	0.040	0.001	-0.008	0.009	2.5	2.4
	300	0.013	0.040	0.001	-0.008	0.009	2.5	2.4
C1S–I2S•••Cl1–Pt1	100	0.016	0.048	0.001	-0.011	0.011	3.5	3.0
	150	0.016	0.048	0.001	-0.011	0.011	3.5	3.0
	200	0.016	0.047	0.001	-0.010	0.011	3.1	3.0
	250	0.015	0.046	0.001	-0.010	0.011	3.1	3.0
	300	0.015	0.045	0.001	-0.010	0.010	3.1	2.7
C1S–I3S•••Cl1–Pt1	100	0.007	0.024	0.001	-0.004	0.005	1.3	1.4
	150	0.007	0.023	0.001	-0.004	0.005	1.3	1.4
	200	0.007	0.022	0.001	-0.004	0.005	1.3	1.4
	250	0.007	0.021	0.001	-0.003	0.004	0.9	1.1
	300	BCP is not found						
C1S–I3S•••Pt1	100	0.010	0.025	0.001	-0.005	0.006	1.6	1.6
	150	0.010	0.025	0.001	-0.005	0.005	1.6	1.4
	200	0.009	0.024	0.001	-0.004	0.005	1.3	1.4
	250	0.009	0.023	0.001	-0.004	0.005	1.3	1.4
	300	0.009	0.022	0.001	-0.004	0.005	1.3	1.4

[a] $E_{int} = -V(\mathbf{r})/2$[8]

[b] $E_{int} = 0.429G(\mathbf{r})$[9]

We observed the I•••Cl bond cleavage upon the temperature increase and at 300 K appropriate BCP disappear; the other bonds are also rather expectedly weakened. Moreover, starting from 250 K ring critical point (3, +1) for the 3-membered cycle $(I^a\cdots Cl–Pt^b)^{a\cdots b}$ were not located. These data collaterally suggest thermally induced $HI_2C–I\cdots\eta^2(Pt–Cl) \rightarrow HI_2C–I\cdots\eta^1{}_{(Pt)}$ transformation.

TH3. Computational Details

The single point calculations for model clusters have been carried out at DFT level of theory using the M06 functional[10] (this functional describes reasonably weak dispersion forces and non-covalent interactions) with the help of Gaussian-09[11] program package. The experimental

X-ray geometries were used as starting points. The Douglas–Kroll–Hess 2nd order scalar relativistic calculations requested relativistic core Hamiltonian were carried out using DZP-DKH basis sets[12-18] for all atoms. The topological analysis of the electron density distribution with the help of the atoms in molecules (AIM) method developed by Bader[19] has been performed by using the Multiwfn program (version 3.3.4).[20]

PART 3. EXPERIMENTAL DATA

EX1. Synthetic work and characterization

Materials and Instrumentation. Solvents, iodoform, KBr, $K_2[PtCl_4]$, and dialkylcyanamides $NCNR_2$ (R_2 = Me_2, Et_2, $(CH_2)_4$, $(CH_2)_5$) were obtained from commercial sources and used as received. The complexes *trans*-$[PtCl_2(NCNR_2)_2]$ (R_2 = Me_2 **1a**, Et_2 **2**, $(CH_2)_5$ **4**) were obtained as previously described.[1, 2] Elemental analyses were performed on 185B Carbon Hydrogen Nitrogen Analyzer Hewlett Packard instrument. Electrospray ionization mass spectra were measured on a Bruker micrOTOF spectrometer equipped with electrospray ionization (ESI) source and MeOH was used as the solvent. The instrument was operated both in positive and negative ion mode using a *m*/*z* range of 50–3000. The capillary voltage of the ion source was set at –4500 V (ESI^+-MS) or 3500 V (ESI^--MS) and the capillary exit at ±(70–150) V. The nebulizer gas flow was 0.4 bar and the drying gas flow 4.0 L•min^{-1}. In the isotopic pattern, the most intensive peak is reported. Infrared spectra (4000–250 cm^{-1}) were recorded on a Shimadzu IR Prestige-21 instrument in KBr pellets. TLC was done on Merck 60 F_{254} SiO_2 plates. ^1H, and $^{13}C\{^1H\}$ NMR spectra were measured on a Bruker-DPX 400 spectrometer at ambient temperature.

Synthesis of *trans*-$[PtBr_2(NCNMe_2)_2]$ (1b). Solid KBr (250.0 mg, 2.10 mmol) was added to a solution of $[PtCl_2(NCNMe_2)_2]$ (28.7 mg, 0.07 mmol) in acetone (10 mL) at 20–25 °C, and the reaction mixture was stirred at

RT for ca. 7 d. The formed yellow suspension was evaporated *in vacuo* to dryness at 40 °C. The product was extracted with three 1-mL portions of CH_2Cl_2. The resulting bright yellow solution was filtered off to remove some insoluble material; the filtrate was evaporated at room temperature to dryness and purified by column chromatography on SiO_2 (eluent $CHCl_3$:ethyl acetate = 8:1, v/v). Yield is 24.3 mg (70%).

1b. Anal. Calcd for $C_6H_{12}N_4Br_2Pt$: C, 14.56; H, 2.44; N, 11.32. Found: C, 14.59; H, 2.39; N, 11.29%. HRESI$^+$-MS, *m/z*: 518.8920 ($[M + Na]^+$, calcd 518.8926), 534.8658 ($[M + K]^+$, calcd 534.8665). TLC: $R_f = 0.50$ (eluent $CHCl_3$:ethyl acetate = 8:1, v/v). IR (KBr, selected bands, cm^{-1}): 2910 (w), ν(C−H); 2296 (m), ν(C≡N). ^1H NMR ($CDCl_3$, δ): 3.00 (s, 12H). $^{13}C\{^1H\}$ NMR ($CDCl_3$, δ): 116.40 (br, C≡N), 40.05 (CH_3). Crystals suitable for X-ray study were obtained by slow evaporation of chloroform solution of **1b**.

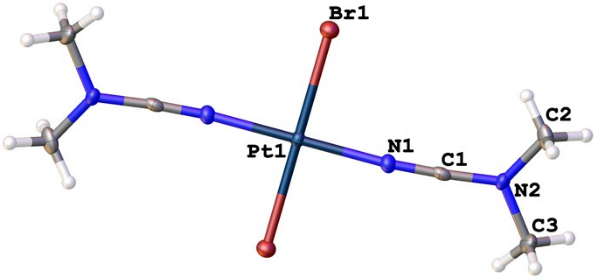

Figure 11S. View of **1b** with the atom numbering scheme. Thermal ellipsoids are shown at the 50% probability level.

Synthesis of *trans*-[PtCl$_2${NCN(CH$_2$)$_4$}$_2$] (3). $NCN(CH_2)_4$ (0.200 ml, 1.98 mmol) was added to $K_2[PtCl_4]$ (0.150 g, 0.36 mmol) in water (5 mL) at room temperature. A yellow powdered precipitate start to release right after the mixing the reactants. It was filtered off after 6 h, washed with three 3-mL portions of water, three 3-mL portions of diethyl ether, and dried in air at room temperature. The *trans* isomer was separated by column chromatography on silica gel (Merck 60 F254, CH_2Cl_2:ethyl acetate = 10:1, v/v, the first fraction). Yield is 99.8 mg (61%).

3. Anal. Calcd for $C_8H_{16}N_4Cl_2Pt$: C, 26.21; H, 3.52; N, 12.23. Found: C, 26.30; H, 3.70; N, 11.92%. HRESI$^+$-MS, *m/z*: 481.0247 ($[M + Na]^+$, calcd 481.0249), 939.0614 ($[2M + Na]^+$, calcd 939.0600). TLC: $R_f = 0.55$ (eluent CH_2Cl_2:ethyl acetate = 10:1, v/v). IR (KBr, selected bands, cm^{-1}): 2975 (w), 2889 (w), *ν*(C−H); 2281 (s), *ν*(C≡N); 336 (w), *ν*(Pt−Cl). ^{1}H NMR ($CDCl_3$, *δ*): 3.58 (m, 4H, NCH_2CH_2), 1.94 (m, 4H NCH_2CH_2). $^{13}C\{^1H\}$ NMR ($CDCl_3$, *δ*): 113.08 (C≡N), 50.59 (NCH_2CH_2), 25.75 (NCH_2CH_2).

EX2. Crystal growth and XRD experiments

Table 13S. Crystallography data and refinement parameters for single-temperature structure studies.

	1a·2CHI$_3$	**1a**·½CHCl$_3$·1½CHI$_3$	**1b**	**1b**·2CHI$_3$	**2**·2CHI$_3$	**3**·2CHI$_3$	**4**·2CHI$_3$
Formula	$C_8H_{14}Cl_2I_6N_4Pt$	$C_{16}H_{28}Cl_7I_9N_8Pt_2$	$C_6H_{12}Br_2N_4Pt$	$C_8H_{14}Br_2I_6N_4Pt$	$C_{12}H_{22}Cl_2I_6N_4Pt$	$C_{12}H_{18}Cl_2I_6N_4Pt$	$C_{14}H_{22}Cl_2I_6N_4Pt$
Mass	1193.62	2112.89	495.11	1282.54	1249.72	1245.69	1273.74
T, K	120	100	100	120	100	100	100
Crystal system	Triclinic	Triclinic	Monoclinic	Triclinic	Triclinic	Monoclinic	Triclinic
Space group	P-1	P-1	P2$_1$/c	P-1	P-1	P2$_1$/c	P-1
Z (Z’)	2 (1)	2 (1)	4 (0.5)	2 (1)	2 (0.5)	4 (0.5)	2 (0.5)
a, Å	9.2555(4)	9.2558(6)	5.7573(4)	9.2800(6)	8.2473(6)	9.9496(3)	9.1290(8)
b, Å	9.6136(4)	9.3667(7)	11.8165(6)	9.8201(6)	8.7723(6)	9.35436(18)	9.1612(8)
c, Å	15.3533(7)	15.2697(11)	9.2197(7)	15.7209(10)	11.3779(6)	14.6232(4)	10.0487(8)
α, °	81.5317(9)	75.799(6)	90	81.0370(13)	104.013(5)	90	100.776(7)
β, °	75.7689(9)	81.826(6)	108.047(8)	75.8368(13)	98.930(5)	103.295(2)	113.593(8)
γ, °	65.7138(8)	65.210(7)	90	65.7179(12)	116.223(7)	90	107.793(8)
V, Å^3	1205.36(9)	1163.95(15)	596.37(7)	1263.74(14)	683.18(9)	1324.53(5)	685.70(11)
d_{calc}, g·cm^{-3}	3.289	3.014	2.757	3.370	3.038	3.123	3.085
F(000)	1040	932	448	1112	552	1096	564
$2\theta_{max}$, °	58	59	60	58	60	68	60
Reflns measured	19998	20329	5140	15799	8627	34242	5774
Independent reflns	6397	5932	1592	6724	4812	5325	3479
Reflns with I>2σ(I)	5361	5152	1303	5849	3978	4868	2917
R_1 (for reflns with I>2σ(I))	0.0322	0.0300	0.0328	0.0351	0.0300	0.0226	0.0345
wR_2 (for all independent reflns)	0.0738	0.0609	0.0710	0.0908	0.0701	0.0479	0.0719
GOF	1.026	1.206	1.066	1.041	1.029	1.098	1.031
Residual electron density, e·Å^{-3}(d_{min}/d_{max})	1.672/-0.790	1.699/-1.952	1.988/-2.254	1.794/-1.278	1.959/-1.060	1.325/-1.270	1.322/-1.818

Table 14S. Crystallography data and refinement parameters for the VT XRD study of **4**•2CHI$_3$.

T, K	100	150	200	250	300
Formula	$C_{14}H_{22}Cl_2I_6N_4Pt$				
Mass	1273.74				
Crystal system	Triclinic				
Space group	P-1				
Z (Z’)	2 (0.5)				
a, Å	9.1465(11)	9.1680(15)	9.1724(12)	9.1743(13)	9.1580(14)
b, Å	9.1681(11)	9.1918(15)	9.2419(12)	9.2939(12)	9.3355(14)
c, Å	10.0680(12)	10.1090(16)	10.1625(13)	10.2287(14)	10.2955(16)
α, °	113.589(2)	113.897(3)	114.172(2)	114.480(2)	114.801(3)
β, °	100.676(2)	100.373(3)	100.036(2)	99.652(2)	99.221(3)
γ, °	107.808(2)	107.948(3)	108.096(2)	108.236(2)	108.383(3)
V, Å^3	689.33(14)	693.9(2)	700.48(16)	707.88(17)	713.19(19)
d_{calc}, g·cm^{-3}	3.068	3.048	3.020	2.988	2.966
F(000)	564	564	564	564	564
$2\theta_{max}$, °	50	50	50	50	50
Reflns measured	7195	7282	7371	7400	7566
Independent reflns	3321	3348	3378	3410	3443
Reflns with I>2σ(I)	2732	2623	2571	2510	2449
R_1 (for reflns with I>2σ(I))	0.0302	0.0333	0.0344	0.0344	0.0348
wR_2 (for all independent reflns)	0.0693	0.0749	0.0798	0.0785	0.0792
GOF	1.005	0.961	0.990	1.024	1.040
Residual electron density, e·Å^{-3}(d_{min}/d_{max})	1.456/-0.970	1.571/-1.404	1.926/-1.053	1.525/-1.016	1.236/-0.776

Table 15S. Crystallography data and refinement parameters for the reversibility confirmation XRD study of **4**•2CHI$_3$.

T, K	100 (first)	300	100 (second)
Formula	$C_{14}H_{22}Cl_2I_6N_4Pt$		
Mass	1273.74		
Crystal system	Triclinic		
Space group	P-1		
Z (Z')	2 (0.5)		
a, Å	9.1654(5)	9.1806(11)	9.1564(6)
b, Å	9.1839(8)	9.3566(9)	9.1703(8)
c, Å	10.0995(10)	10.3153(10)	10.0589(8)
α, °	113.841(9)	114.930(9)	113.561(7)
β, °	100.430(6)	99.180(10)	100.692(7)
γ, °	108.001(7)	108.364(10)	107.883(7)
V, Å^3	692.27(11)	717.26(14)	689.26(10)
d_{calc}, g·cm^{-3}	3.055	2.949	3.069
F(000)	564	564	564
$2\theta_{max}$, °	50	50	50
Reflns measured	8875	5354	6577
Independent reflns	3928	3528	3816
Reflns with $I>2\sigma(I)$	3051	2422	3177
R_1 (for reflns with $I>2\sigma(I)$)	0.0379	0.0420	0.0391
wR_2 (for all independent reflns)	0.0915	0.1042	0.0924
GOF	1.096	1.028	1.071
Residual electron density, e·Å^{-3}(d_{min}/d_{max})	1.503/-1.522	0.991/-1.388	2.710/-2.634

Single crystals of **1b** were grown by slow evaporation of chloroform solution. Crystals of the associates suitable for X-ray diffraction studies were obtained by slow evaporation of solvents (chloroform for **1a**•½CHCl$_3$•1½CHI$_3$, **2**•2CHI$_3$, **3**•2CHI$_3$ and **4**•2CHI$_3$ and dichloromethane for **1a**•2CHI$_3$ and **1b**•2CHI$_3$) from solutions of complex:iodoform = 1:2 mixture at 20–25 °C *in the dark* to prevent light-induced iodoform decomposition.

All XRD studies were performed using graphite-monochromated MoKα radiation and ω-scan regime: X-ray diffraction data for crystals of **1a**•½CHCl$_3$•1½CHI$_3$, **1b**, **2**•2CHI$_3$, **3**•2CHI$_3$ and **4**•2CHI$_3$ were collected using an Oxford Diffraction Xcalibur diffractometer (at 100K), whereas XRD studies of **1a**•2CHI$_3$ and **1b**•2CHI$_3$ (at 120K) as well as VT XRD studies of **4**•2CHI$_3$ (100–300K; 50K step) were performed on a Bruker APEX II Duo diffractometer. For **4**•2CHI$_3$ several crystals from different samples were studied to make more statistically significant the observation of the bifurcated bonding. On the contrary, one single-set crystal of **4**•2CHI$_3$ was used for the VT XRD study to prevent possible experimental inaccuracies.

X-ray absorption effects are accounted for by empirical corrections based on measurements of equivalent reflections. All structures were solved by direct methods and refined against F^2_{hkl} by least-squares technique using full-matrix anisotropic approximation for non-hydrogen atoms. Hydrogen atom positions were always calculated using geometric criteria; all hydrogen atoms were refined in riding model within the isotropic approximation.

The disorder within one independent half of the complex molecule in **1a**•2CHI_3 and **1b**•2CHI_3 were modeled by the free-populated superposition of two sets of the NMe_2 group coordinates corresponding to slightly different rotations around the C1–N2 bond. The replacement disorder of one iodoform molecule in **1a**•½$CHCl_3$•1½CHI_3 was identified by the analysis of geometry data (the C–I bond lengths) and anisotropic displacement parameters; both indicate the incomplete populations of the I4S, I5S and I6S atoms. Further modeling of a half of each of these three positions by chlorine scattering factor led to reasonable displacement parameters and decrease *R*-values; however, due to unfeasible geometry derived from free-coordinate refinement, the C–I and C–Cl bond lengths were then restrained on 2.15 and 1.75 Å values with 0.02 Å uncertainties. Note that the modelling of the NMe_2 disorder in **1a**•½$CHCl_3$•1½CHI_3 provide structurally unreasonable results, probably due to significant increase of refinement parameters in that case.

In order to confirm the reversibility of thermal transformations of the **4**•2CHI_3 structure, three additional XRD datasets were collected at 100 K, 300 K and again at 100 K using one crystal single-set on an Oxford Diffraction Xcalibur diffractometer. Taking into account uncertainties of low-temperature device as well as least-squares refinement uncertainties crystal structure was found nearly the same before and after heating to 300 K. Collected data argue for the independence of thermally induced crystal structure variation on the direction of temperature changing, that is common for a crystal structure which within some temperature regime do not undergo phase transitions and are exposed to thermal expansion only.

Crystallography data and parameters of final refinements are listed in **Tables 13S–15S**. All calculations were done using CrysAlisPro[21]/Olex2[22] tandem for the **1a**•½$CHCl_3$•1½CHI_3, **1b**, **2**•2CHI_3, **3**•2CHI_3, and **4**•2CHI_3 and

Bruker APEX3[23]/ShelXS[24]/ShelXL[25] software packages for the **1a**•$2CHI_3$ and **1b**•$2CHI_3$ and VT XRD data for **4**•$2CHI_3$.

References

1. N. A. Bokach, T. B. Pakhomova, V. Y. Kukushkin, M. Haukka and A. J. L. Pombeiro, *Inorganic Chemistry*, 2003, **42**, 7560-7568.
2. P. V. Gushchin, N. A. Bokach, M. Haukka, E. S. Dmitrieva and V. Y. Kukushkin, *Acta Crystallographica Section E*, 2006, **62**, m244–m246.
3. L. Brammer, G. M. Espallargas and H. Adams, *Crystengcomm*, 2003, **5**, 343–345.
4. E. Arunan, G. R. Desiraju, R. A. Klein, J. Sadlej, S. Scheiner, I. Alkorta, D. C. Clary, R. H. Crabtree, J. J. Dannenberg, P. Hobza, H. G. Kjaergaard, A. C. Legon, B. Mennucci and D. J. Nesbitt, *Pure Appl. Chem.*, 2011, **83**, 1637-1641.
5. G. R. Desiraju, P. S. Ho, L. Kloo, A. C. Legon, R. Marquardt, P. Metrangolo, P. Politzer, G. Resnati and K. Rissanen, *Pure Appl. Chem.*, 2013, **85**, 1711–1713.
6. F. Allen, *Acta Crystallographica Section B*, 2002, **58**, 380–388.
7. F. Bertolotti and G. Gervasio, *J. Mol. Struct.*, 2013, **1036**, 305-310.
8. E. Espinosa, E. Molins and C. Lecomte, *Chem. Phys. Lett.*, 1998, **285**, 170–173.
9. M. V. Vener, A. N. Egorova, A. V. Churakov and V. G. Tsirelson, *J. Comput. Chem.*, 2012, **33**, 2303–2309.
10. Y. Zhao and D. G. Truhlar, *Theor. Chem. Acc.*, 2008, **120**, 215–241.
11. M. J. Frisch, G. W. Trucks, H. B. Schlegel, G. E. Scuseria, M. A. Robb, J. R. Cheeseman, G. Scalmani, V. Barone, B. Mennucci, G. A. Petersson, H. Nakatsuji, M. Caricato, X. Li, H. P. Hratchian, A. F. Izmaylov, J. Bloino, G. Zheng, J. L. Sonnenberg, M. Hada, M. Ehara, K. Toyota, R. Fukuda, J. Hasegawa, M. Ishida, T. Nakajima, Y. Honda, O. Kitao, H. Nakai, T. Vreven, M. J. A.;, J. E. Peralta, F. Ogliaro, M. Bearpark, J. J. Heyd, E. Brothers, K. N. Kudin, V. N. Staroverov, T. Keith, R. Kobayashi, J. Normand, K. Raghavachari, A. Rendell, J. C. Burant, S. S. Iyengar, J. Tomasi, M. Cossi, N. Rega, J. M. Millam, M. Klene, J. E. Knox, J. B. Cross, V. Bakken, C. Adamo, J. Jaramillo, R. Gomperts, R. E. Stratmann, O. Yazyev, A. J. Austin, R. Cammi, C. Pomelli, J. W. Ochterski, R. L. Martin, K. Morokuma, V. G. Zakrzewski, G. A. Voth, P. Salvador, J. J. Dannenberg, S. Dapprich, A. D. Daniels, O. Farkas, J. B. Foresman, J. V. Ortiz, C. J.; and D. J. Fox, *Gaussian 09, Revision C.01*, Gaussian, Inc., Wallingford, CT, **2010**.
12. C. L. Barros, P. J. P. de Oliveira, F. E. Jorge, A. C. Neto and M. Campos, *Mol. Phys.*, 2010, **108**, 1965-1972.
13. F. E. Jorge, A. C. Neto, G. G. Camiletti and S. F. Machado, *J. Chem. Phys.*, 2009, **130**, 6.
14. A. C. Neto and F. E. Jorge, *Chem. Phys. Lett.*, 2013, **582**, 158-162.
15. R. C. de Berredo and F. E. Jorge, *Journal of Molecular Structure - Theochem*, 2010, **961**, 107–112.
16. C. L. Barros, P. J. P. de Oliveira, F. E. Jorge, A. C. Neto and M. Campos, *Mol. Phys.*, 2010, **108**, 1965–1972.
17. F. E. Jorge, A. C. Neto, G. G. Camiletti and S. F. Machado, *J. Chem. Phys.*, 2009, **130**, 064108.
18. A. C. Neto and F. E. Jorge, *Chem. Phys. Lett.*, 2013, **582**, 158–162.
19. R. F. W. Bader, *Atoms in Molecules: A Quantum Theory, Oxford University Press, Oxford*, 1990.

20. T. Lu and F. W. Chen, *J. Comput. Chem.*, 2012, **33**, 580–592.
21. CrysAlisPro: Agilent (2014). *CrysAlis PRO*. Agilent Technologies Ltd, Yarnton, Oxfordshire and England.
22. O. V. Dolomanov, L. J. Bourhis, R. J. Gildea, J. A. K. Howard and H. Puschmann, *J. Appl. Cryst.*, 2009, **42**, 339-341.
23. Bruker (2012). *APEX3*. Bruker AXS Inc., Madison, Wisconsin and USA.
24. G. M. Sheldrick, *Acta Crystallogr. Sect. A*, 2008, **64**, 112-122.
25. G. M. Sheldrick, *Acta Crystallographica Section C*, 2015, **71**, 3–8.